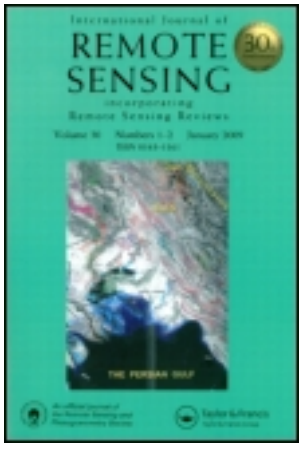

International Journal of Remote Sensing

Publication details, including instructions for authors and subscription information:
http://www.tandfonline.com/loi/tres20

Remote sensing of snow - a review of available methods

Andreas Juergen Dietz [a], Claudia Kuenzer [a], Ursula Gessner [a] & Stefan Dech [a]

[a] German Remote Sensing Data Center (DFD), German Aerospace Center (DLR), Wessling, Germany

Published online: 13 Dec 2011.

To cite this article: Andreas Juergen Dietz , Claudia Kuenzer , Ursula Gessner & Stefan Dech (2012): Remote sensing of snow - a review of available methods, International Journal of Remote Sensing, 33:13, 4094-4134

To link to this article: http://dx.doi.org/10.1080/01431161.2011.640964

International Journal of Remote Sensing
Vol. 33, No. 13, 10 July 2012, 4094–4134

Taylor & Francis
Taylor & Francis Group

Review Article

Remote sensing of snow – a review of available methods

ANDREAS JUERGEN DIETZ*, CLAUDIA KUENZER, URSULA GESSNER and STEFAN DECH

German Remote Sensing Data Center (DFD), German Aerospace Center (DLR), Wessling, Germany

(*Received 21 March 2011; in final form 19 August 2011*)

The use of satellite remote sensing for the mapping of snow-cover characteristics has a long-lasting history reaching back until the 1960s. Because snow cover plays an important role in the Earth's climate system, it is necessary to map snow-cover extent and snow mass in both high temporal and high spatial resolutions. This task can only be achieved by the use of remotely sensed data. Many different sensors have been used in the past decades with various algorithms and respective accuracies. This article provides an overview of the most common methods. The limitations, advantages and drawbacks will be illustrated while error sources and strategies on how to ease their impact will be reviewed. Beginning with a short summary of the physical and spectral properties of snow, methods to map snow extent from the reflective part of the spectrum, algorithms to estimate snow water equivalent (SWE) from passive microwave (PM) data and the combination of both spectra will be delineated. At the end, the reader should have an overarching overview of what is currently possible and the difficulties that can occur in the context of snow-cover mapping from the reflective and microwave parts of the spectrum.

1. Introduction

Snow cover plays an important role both globally and regionally as it reflects a large portion of the insolation, therefore keeping the Earth's radiation budget in balance (Klein *et al*. 2000, Jain *et al*. 2008, Zhao and Fernandes 2009). Approximately 40–50% of the Northern Hemisphere is covered with snow during midwinter (Hall *et al*. 1995, Pepe *et al*. 2005, Lemke *et al*. 2007), making snow cover the most prevalent land-cover type during the season. On a regional scale, snow cover is important for local water availability, river run-off and groundwater recharge, especially in middle and high latitudes (Akyürek and Sorman 2002, Jain *et al*. 2008). In countries such as Norway or Switzerland, where electricity is mainly generated through hydropower stations, snow cover plays a relevant role in energy supply (Vikhamar and Solberg 2003). In this context, exact knowledge of the snow-covered area is also essential for water resource management, for example when using snowmelt runoff models (Butt and Bilal 2011). Also, information about the water equivalent of snow is important for hydrological modelling and water resource management (Foster *et al*. 2005). Furthermore, it is reported that changes in winter snow depth (SD) influence the vegetation growth of certain land-cover types (Peng *et al*. 2010).

*Corresponding author. Email: andreas.dietz@dlr.de

International Journal of Remote Sensing
ISSN 0143-1161 print/ISSN 1366-5901 online
http://www.tandf.co.uk/journals
http://dx.doi.org/10.1080/01431161.2011.640964

A decrease in snow-covered areas has been observed globally since the 1960s, when satellites first started to monitor the Earth's surface (Brown 2000, Lemke *et al*. 2007). In some regions such as China, a trend of increasing snow cover has been observed (from 1978 to 2006 (Che *et al*. 2008), from 1951 to 1997 (Qin *et al*. 2006)). Climate change influences the global snow-cover conditions as it leads to earlier melting and less area coverage (Foster *et al*. 1996). Parameters such as SD may also increase because of high temperatures, depending on the geographic location. While SD decreases south of 40° N, it is reported to increase north of 40° N (Peng *et al*. 2010). Brown (2000) analysed SD and climate data time series and corroborated this trend. Precipitation in the Northern Hemisphere increases up to 4%, thus causing increased snow accumulation during cold months and a reduced snow accumulation during spring. This trend was also reported by Ye *et al*. (1998), where SD data for the whole of Russia were investigated. Between 50–70° N and 30–140° E, a significant SD increase was found for the period from 1936 to 1986. For the complete Northern Hemisphere, however, the mean monthly snow-cover extent decreases by 1.3% per decade (Barry *et al*. 2007). In this context, it is important to map snow-cover and SD changes in both high temporal and high areal coverage, which can only be conducted with remotely sensed data.

This article presents the recent research developments in snow-cover mapping followed by the earlier reviews undertaken by Hall and Martinec (1985), Bernier (1987), Rott (1987), Lucas and Harrison (1990), Massom (1991), König *et al*. (2001), Solberg *et al*. (2006) and Amlien (2008). This article aims to compare the common methods for optical, passive microwave (PM) and synthetic aperture radar (SAR) data and their respective advantages and drawbacks in recognizing snow extent, SD and snow water equivalent (SWE).

2. Physical and spectral properties of snow and their usability for analysing remotely sensed data

Spectral reflectivity and scattering characteristics of snow depend on many different factors such as snow grain size and shape, liquid water content, SD, impurity of snow, temperature, ice content, depth hoar (result of snow metamorphism from low to moderate density; Domine *et al*. 2007) and the consistency of the surface beneath the snow cover (Hall and Martinec 1985, Sturm *et al*. 1995, Tait 1998, Kelly *et al*. 2003, Foster *et al*. 2005, Painter *et al*. 2009). Depending on the chosen sensor type and resolution, the interference of all these factors on the retrieval of snow parameters may vary. The following subsections will outline the details.

2.1 *Snow in the reflective part of the electromagnetic spectrum (0.4–3 μm)*

Snow reflects a high proportion of the radiation in visible (VIS) wavelengths. Depending on the impurity, grain size and age of the snow, this proportion can reach 80% (Winther *et al*. 1999, Klein *et al*. 2000, König *et al*. 2001) to 90% (Hall and Martinec 1985) for freshly fallen, pure snow. With high snow age, the percentage of reflected insolation decreases. The reasons for this decrease arise from various facts. First, the impurity of the snowcover increases with time, leading to decreased reflectance. Aoki *et al*. (2000) suggested that the fallout of atmospheric aerosols is the main contributor to the impurity of the snow surface. Aoki *et al*. (2007) measured the impurity of different snow stages and found impurity concentrations of 2–8 parts per million by weight (ppmw) during accumulation period and up to 100 ppmw and

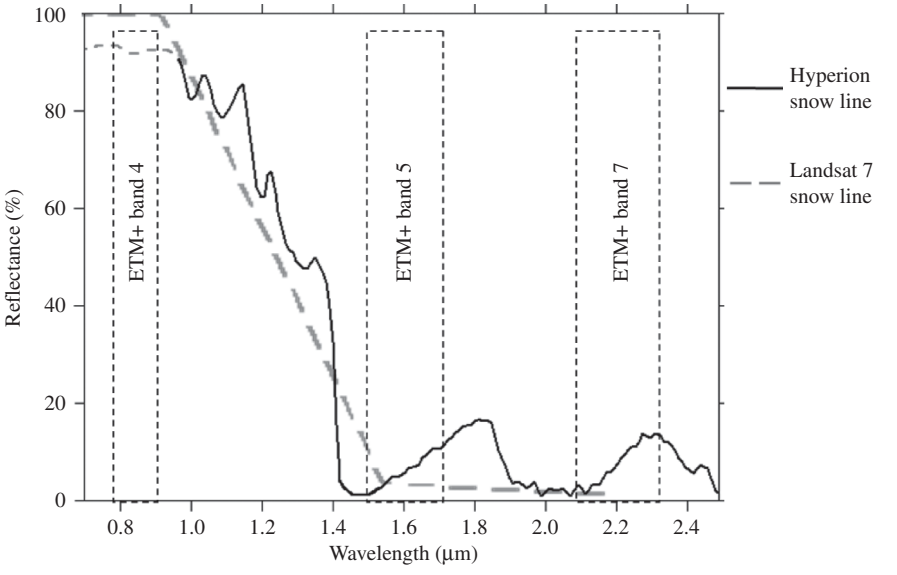

Figure 1. Reflectance of snow derived from Hyperion. The wavelength region ahead of 1.0 μm is not functional and has been replaced with values from Dozier (1989).

more during the melt period. Secondly, melting and refreezing processes within the snow lead to an increased grain size, which then leads to reduced reflectance (Hall and Martinec 1985, Rango 1996, Foster *et al*. 1999).

For longer wavelengths, the reflectance of snow declines significantly, reaching near-zero values in the region of the near-infrared (IR) (Pepe *et al*. 2005, Wang *et al*. 2005). Figure 1 shows a typical reflectance curve of snow derived from the hyperspectral Hyperion sensor. This sensor uses 220 unique spectral bands covering wavelengths of 0.35–2.57 μm at a spatial resolution of 30 m (Griffin *et al*. 2005). The observed spectra of Hyperion and Landsat 7, also shown in figure 1, are similar, but the wide range of individual bands permits detailed analysis of the spectral behaviour of surface features such as – in this case – snow. The displayed spectrum is that of the snow of Central Kyrgyzstan near Lake Song-Kul, recorded on 29 December 2002. The wavelength region ahead of 1.0 μm in figure 1 (grey dotted line) is not available from Hyperion. Therefore, values from Dozier (1989) have been integrated into the figure. Note that the age of the observed snowpack from the Hyperion scene was unknown. The slight differences between the measured reflectance and the modelled values may be caused by impurities, vegetation or liquid water content. This demonstrates that the modelled reflectance curves differ from the actual satellite measurements.

The low spectral resolution of Landsat 7 (acquisition date: 5 March 2002) and the saturation of the VIS channels make it more difficult to recognize the distinctive features that characterize snow.

Different grain sizes lead to high variability in the reflection properties of snow, especially in regions around 1 and 1.2–1.3 μm, whereas the characteristics remain similar in the region below 0.8 and 1.5 μm (Hall and Martinec 1985, Dozier 1989, König *et al*. 2001). Figure 2 shows the influence of snow grain size on the reflectance of snow. While in the VIS part of the spectrum the differences of the signatures are

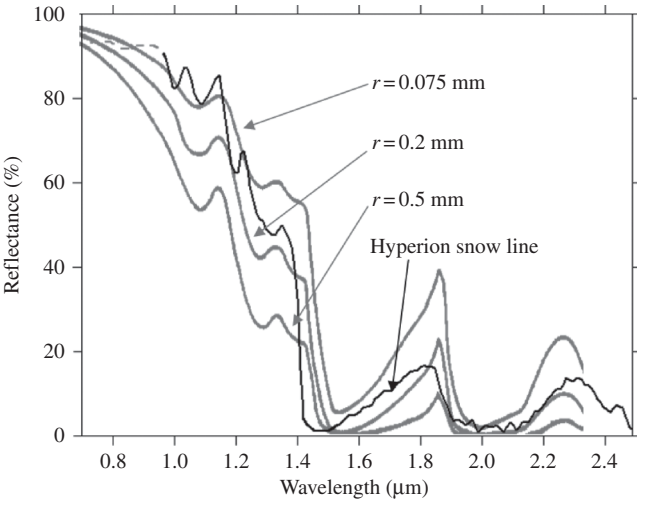

Figure 2. Influence of different snow grain sizes (r) on the reflectance of snow. The black spectral signature was again derived from Hyperion, the grey signatures have been adopted and modified from Choudhury and Chang (1979).

small, the differences increase for longer wavelengths with a maximum in the region from 0.95 to 1.40 μm. For a detailed description of the spectral reflectance of snow and how the optical depth of a snowpack can be calculated, refer to Dozier (1989).

As mentioned above, impurity and age of snow can also influence the spectral behaviour. Figure 3 gives an example of the spectral behaviour of different snow and ice surfaces for the range 0.4–1.2 μm. Fresh snow reflects up to 100% in this figure, which was adopted and modified from Zeng *et al*. (1984). While a snowpack ages, the amount of reflected radiation decreases. For ice surfaces, this amount is further reduced, reaching a minimum for dirty glacier ice with only 15–20% reflection. The measurements given in figure 3 have been collected from a study area in North China from 1980 to 1982, using a spectral radiometer with a wavelength range of 0.38–1.20 μm and a spectral resolution of 0.01 μm. The snowpack can change its spectral characteristics considerably within even a few hours. Figure 4 shows this behaviour for the same study area in North China, derived from Zeng *et al*. (1984). For signatures A and B in figure 4, the temperature was below 0°C and the time span between the measurements was 40 hours. Although air temperatures were below freezing point, the snow had undergone slight snow crystal metamorphosis, increasing snow grain size and snowpack density and therefore altering the reflection for up to 10% in the IR region. Signatures C, D and E refer to slightly wet, wet and water saturated snowpacks, respectively (Zeng *et al*. 1984).

One of the major challenges in snow mapping is the discrimination between clouds and snow. Although other land-cover classes can be easily discriminated from clouds in the VIS wavelengths, snow may behave similarly to clouds in the reflective and thermal part of the spectrum (Akyürek and Sorman 2002, Miller and Lee 2005, Wang *et al*. 2005, Hyvärinen *et al*. 2009, Hall *et al*. 2010). Figure 5 gives an example of spectral signatures for different clouds (r = particle radii) and snow.

The major differences between the reflective characteristics of clouds and snow have been described by Dozier (1989); water drops (10 μm) or ice crystals (40 μm) within

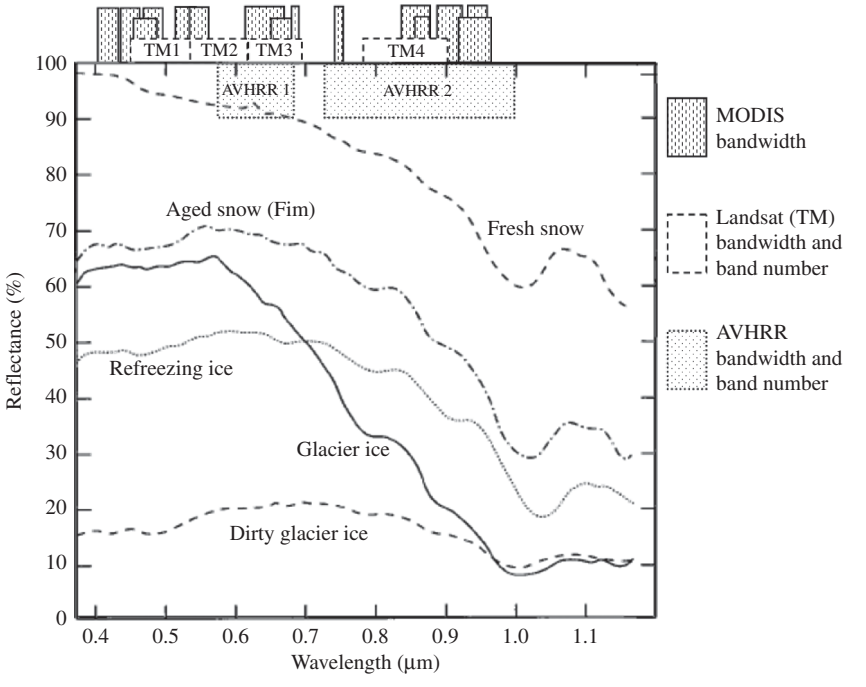

Figure 3. Reflectance of different surface types related to snow cover. The bandwidths of Landsat (TM), MODIS (M) and AVHRR are also integrated (Zeng *et al*. 1984, modified).

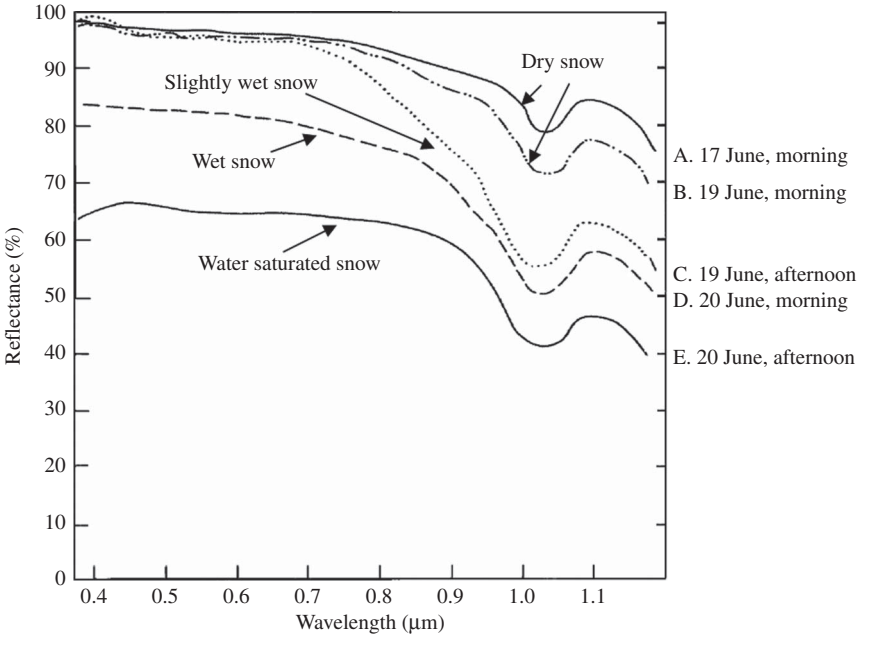

Figure 4. Reflectance of different snow age and wetness stages (Zeng *et al*. 1984, modified).

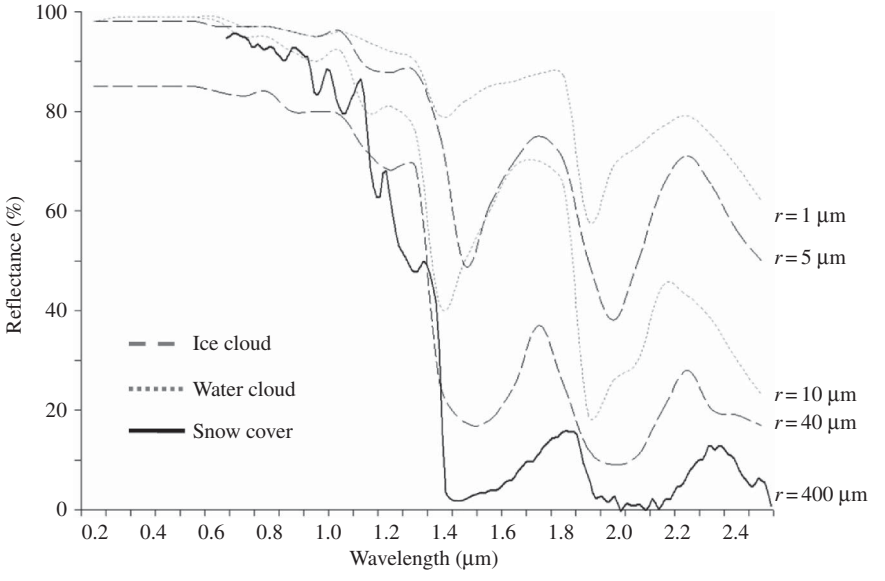

Figure 5. Spectral behaviour of different cloud types compared to snow (Dozier 1989, modified).

clouds are smaller than typical snow grains (300–500 μm, Chang *et al*. 1987). The smaller particle size and the water content cause less absorption in the spectral region from 1.55 to 1.70 μm (Hall *et al*. 2002, Pepe *et al*. 2005). However, ice-containing clouds cannot be discriminated from snow by this feature. Because snow cover is usually optically thicker than cloud cover, it reflects a larger proportion of the VIS radiation. This criterion can help to distinguish between thin cirrus clouds and snow.

The characteristic decline of snow reflectance towards short-wave IR can be useful to distinguish between the cloud and snow because most clouds reflect a higher proportion of the short-wave IR (Hall *et al*. 2002, Pepe *et al*. 2005). Sensors such as the Advanced Very High Resolution Radiometer (AVHRR), the Moderate Resolution Imaging Spectroradiometer (MODIS) or Landsat provide the appropriate spectral channels to utilize the properties mentioned above. Table 1 gives an overview of the optical sensors reviewed in §3 and also includes the most relevant characteristics. Usually, using only one spectral channel to discriminate between clouds and snow can lead to errors (Miller and Lee 2005). To identify the low and high, thin and thick, warm and iced clouds correctly and avoid confusion with snow cover, a combination of multiple spectral bands is advisable (King *et al*. 1997, Ackerman *et al*. 2010). But even then, confusion between clouds and snow can occur (Hall *et al*. 2002, Klein and Barnett 2003). If cloud coverage exceeds certain threshold percentages, a satellite scene can become useless for snow detection. Rodell and Houser (2004) have identified a maximum cloud coverage of 94% of an entire MODIS scene to be the upper limit beyond which successful snow-cover delineation is unfeasible.

2.2 *Impacts of snow cover on Earth's microwave emittance*

The Earth continuously emits microwave radiation from its surface that can be measured from space using PM sensors (König *et al*. 2001). Such data have been collected

Table 1. Characteristics of optical sensors used for snow detection.

Satellite/sensor	Operational since/until	Spectral bands (μm)	Spacial resolution (m)	Swath width	Data acquisition
Landsat 1–3/MSS	1972/1983	0.5–0.6, 0.6–0.7, 0.7–0.8, 0.8–1.1	79	185 km	Every 18 days
Landsat 4–5/TM	1982/present	0.45–0.52, 0.52–0.6, 0.63–0.69, 0.76–0.9, 1.55–1.75, 2.08–2.35, 10.4–12.5	30 (band 6: 120)	185 km	Every 16 days
Landsat 7/ETM+	1999/present	0.45–0.52, 0.53–0.6, 0.63–0.69, 0.78–0.9, 1.55–1.75, 2.09–2.35, 10.4–12.5, 0.52–0.9	30 (band 6: 60; band 7: 15)	185 km	Every 16 days
Terra & Aqua/MODIS	2000/present	36 bands from 0.62 to 14.38	Bands 1–2: 250; Bands 3–7: 500; Bands 8–36: 1000	2330 km	2 per day
NOAA/AVHRR	1978/present	0.58–0.68, 0.72–1.0, 1.58–1.64, 3.55–3.93, 10.3–11.3 (10.5–11.5)*, 11.5–12.5**	1090	2399 km	Daily
GOES	1975/present	0.52–0.72, 3.78–40.3, 6.47–7.02, 10.2–11.2, 11.5–12.5	Bands 1: 1000, Bands 2–4: 4000, band 5: 8000	Full Earth disk	Every 3 hours
SPOT/ VEGETATION	1998/present	0.43–0.47, 0.61–0.68, 0.78–0.89, 1.58–1.75	1150	2200 km	1–2 days
ERS-2/ATSR-2	1995/present	0.55, 0.66, 0.87, 1.6, 3.7, 10.8, 12.0	1000	512 km	2–3 days
Envisat/AATSR	2002/present	0.55, 0.66, 0.87, 1.6, 3.7, 11.0, 12.0	1000	500 km	2–3 days
Envisat/MERIS	2002/present	15 bands from 0.39 to 1.04	300	1150 km	2–3 days

Notes: *Valid for AVHRR/2 instead of 10.3–11.3 μm band.
**Only valid for AVHRR/3.

Table 2. Passive microwave sensors and their characteristics.

	SMMR	SSM/I	AMSR-E
Operational since/until	1978/1987	1987/present	2002/present
Platform	Nimbus-7	DMSP	Aqua
Frequencies and IFOV (km × km)	6.6 GHz; 156 × 156	N/A	6.9 GHz; 74 × 43
	10.7 GHz; 97 × 97	N/A	10.6 GHz; 51 × 30
	18.0 GHz; 60 × 60	19.3 GHz; 69 × 43	18.7 GHz; 27 × 16
	21.0 GHz; 60 × 60	22.2 GHz; 60 × 40	23.8 GHz; 31 × 18
	37.0 GHz; 30 × 30	37.0 GHz; 37 × 29	36.5 GHz; 14 × 8
	N/A	85.5 GHz, 15 × 13	89.0 GHz; 6 × 4
Polarizations	H/V	H/V*	H/V
Incidence angle (°)	49	53	53
Data acquisition	Every other day	daily	daily
Swath width	780 km	1400 km	1600 km
Sensitivity (K)	0.9–1.5	0.8–1.1	0.3–1.1

Notes: *22.2 GHz channel is only available in vertical polarization. DMSP, Defense Meteorological Satellite Program.

by the Scanning Multichannel Microwave Radiometer (SMMR), the Special Sensor Microwave/Image (SSM/I) and the Advanced Microwave Scanning Radiometer – Earth Observing System (AMSR-E), thus providing a large and continuous time series on a global scale (see table 2 for details about the sensors).

Snow-covered areas attenuate the emitted microwave radiation from the underlying surface for wavelengths similar to the snow grain size (Chang *et al*. 1987). This attenuation of microwave radiation depends principally on the snow mass of a respective snowpack; the more the snow covers an area, the less the microwave radiation will reach the satellite sensor (Chang *et al*. 1987, König *et al*. 2001, Clifford 2010).

A snowpack consists of air, ice and in some cases liquid water. Because the air does not influence the microwave signal (or at least can be neglected, see Mätzler and Wegmüller 1987, Mätzlar 1994), the propagation of microwaves in a snowpack depends on the dielectric constants of ice and water, which are extremely different. Liquid water content, grain size and grain shape may influence the signal that reaches the sensor (Foster *et al*. 1999, Clifford 2010). For dry snow, the scattering is caused by the dielectric discontinuities of snow grains and air. Microwave absorption within dry snow is low, resulting in volume scattering of the snowpack (Amlien 2008).

PM sensors map the surface in different frequencies and polarizations. Vertically polarized data are more sensitive to the snow volume and are therefore capable of mapping shallow snow cover. However, because there could be a confusion between snow and underlying dry soils, horizontally polarized data are usually used to map snow cover (Grody and Basist 1996, Amlien 2008). The frequency is crucial for the wavelength and the spatial resolution of the signal. The higher the frequency, the finer is the resolution of the resultant pixel, but the wavelength also decreases with increasing frequency.

The maximum SD that can be derived from PM sensors depends on the wavelength of the signal. The 37 GHz channel, for example, which is often used to derive SWE (Chang *et al*. 1987, Josberger and Mognard 2002), has a wavelength of 0.8 cm, limiting the maximum SD that can be measured to 10–100 times the wavelength, thus ~100 cm (Clifford 2010) and a respective SWE of 250 mm (Foster *et al*. 2005). Derksen

(2008) observed that SWE measurements derived from the 37 GHz channel inherit an increasing uncertainty with rising SWE; volume scattering is reduced at SWE values greater than 120 mm. Scattering effects are also decreased when the wavelength of the signal becomes greater than the grain size of the snow crystals. Increasing the wavelength of the sensors will therefore not improve the ability to map deeper snow.

At wavelengths greater than 5 cm, not scattering but absorption will be the dominant process (Chang *et al*. 1987). The minimum SD that can be recognized by PM sensors has been identified at 2 cm (Che *et al*. 2008).

The snow crystal properties can influence the signal and may lead to an overestimation of the SWE. Initially, a fixed snow crystal diameter and snow density was assumed for the calculations, for example, 1 mm crystal size and 300 kg m^{-3} snow density (Rott and Nagler 1995). Large divergences from these fixed values can lead to wrong assumptions. Foster *et al*. (1999) have shown that the shape of the snow crystals has little to no impact on SD and SWE estimations derived from the PM radiometry. The crystal size is a more sensitive factor. Especially in regions with plate-like depth hoar crystals, an overestimation of SWE has been observed (Clifford 2010).

The analysis of PM data is subject to some other major restrictions. Forests tend to mask out the snow cover, leading to underestimation of SD and SWE (Hall *et al*. 1982, Foster *et al*. 1991). The vegetation absorbs microwaves in the 37 GHz region, thereby suppressing the scattering signal emitted from the snow surface underneath (Derksen 2008). Liquid water increases the dielectric losses within the snowpack, which strongly increases the absorption of microwaves within the snowpack. Volume scattering is therefore completely prevented leading to strongly degraded SD estimation (Rott and Nagler 1995, Amlien 2008). Algorithms to estimate SD under wet snow conditions are, therefore, still being researched (Kelly 2009). Furthermore, owing to its coarse resolution, PM data are more suitable for global monitoring of snow properties than it is for a regional scale (Vikhamar and Solberg 2002). Although the resolution may be the biggest disadvantage of PM sensors, their ability to map snow even in the presence of clouds makes them a valuable tool for snow-cover mapping. The possibility to estimate SD and SWE is another big advantage of this sensor type.

2.3 *Interactions between snow cover and active microwave data*

The use of active microwave data to map snow-cover characteristics is limited by the fact that only wet snow can be recognized reliably (Wang *et al*. 2008a). Under dry conditions, it is not the snow crystals but the ground beneath the snow cover that forms the major source for the backscattering signal (König *et al*. 2001). Liquid water reduces the penetration depth of the microwaves from around 20 m in dry conditions to only 13.8 cm with 1% of liquid water content (Rott and Nagler 1994). Active sensors can come with much higher spatial resolutions than PM sensors, reducing swath (50–500 km) and revisit frequency (24 days for RADARSAT SAR, 35 days for Envisat ASAR, 11 days for TerraSAR-X; König *et al*. 2001, Nghiem and Tsai 2001, Strozzi *et al*. 2009).

Ice layers within refrozen snow bodies can be recognized by scatterometers such as QuickSCAT (QSCAT) using the K_u band at 13.4 GHz, as shown by Nghiem *et al*. (2005). Additionally, the beginning of snowmelt can be recognized because of the liquid water content that appears within the snowpack. This feature is exploited in combination with optical and PM sensors by Foster *et al*. (2011) and the same is reviewed in §3. Table 3 gives an overview of the different active microwave sensors and

Table 3. Characteristics of selected active microwave sensors.

Satellite/ sensor	Operational since/until	Bands	Spacial resolution	Swath width	Data acquisition
ADEOS I/ NSCAT	1996/1997	K_u band (14.0 GHz)	50 km	2 × 600 km	Every other day
QuickSCAT/ Seawinds	1999/2009	K_u band (13.4 GHz)	25 km	1800 km	Daily
ADEOS II/ SeaWinds	2002/present	K_u band (13.4 GHz)	25 km	1800 km	Daily
MetOp/ASCAT	2005/present	C band (5.25 GHz)	25 km, 50 km	2 × 550 km	Every other day
RADARSAT/ SAR	1995/present	C band (5.3 GHz)	8–100 m	45–500 km	Every 24 days
RADARSAT2/ SAR	2007/present	C band (5.4 GHz)	3–100 m	20–500 km	Every 24 days
Envisat/ASAR	2001/present	C band (5.3 GHz)	30, 150, 1000 m	60–100, 400 km	Every 35 days
JERS 1/SAR	1992/1998	L band (1.275 GHz)	18 m	75 km	Every 44 days
TerraSAR-X, TanDEM-X/ SAR	2007/present	X band (9.6 GHz)	1, 3, 18 m	10, 50, 150 km	Every 11 days

their characteristics. The interest in analysing the scatterometer data for snow-cover mapping has increased in recent years (Foster *et al*. 2011). However, because the use of active microwave data for snow-cover detection is limited to the existence of liquid water content, methods to use these data are excluded from detailed examination.

3. Methods to map snow extent, snow depth and SWE from remotely sensed data

TIROS-1 (Television and InfraRed Observation Satellite) was the first satellite that enabled mapping of snow cover from space in April 1960 (Lucas and Harrison 1990). Since then, many sensors with various spectral channels and spatial and temporal resolution have been used to improve these first efforts.

The algorithms and methods to map snow parameters from remotely sensed data vary primarily depending on the sensor type, but may also be influenced by the most prevalent land-cover type, topography and climatic conditions. This section gives an overview of the most important methods to map snow extent, SD and SWE. It is not possible to include every single method in a clearly arranged manner, so only the most recent or most commonly applied and published methods are reviewed. Table 4 summarizes the methods discussed in this review. Additional details such as resolution, accuracy of the product and respective authors who investigated the methods are also included.

3.1 *Discrete methods for the identification of snow cover with optical sensors*

In this section, the most prevalent methods to map snow cover from the reflective part of the spectrum are summarized.

Snowmap is an algorithm that was developed especially for MODIS (Hall *et al*. 1995). The MODIS daily, 8-day and monthly snow-cover products provided by the National Snow and Ice Data Center (NSIDC) are based on this algorithm. It uses the reflectance of VIS and IR radiation to calculate the normalized difference snow index (NDSI):

Table 4. Overview of reviewed methods and their characteristics.

Sensor(s)	Method(s)	Author(s)	Spacial resolution	Temporal resolution	Accuracy	Derived parameters
MODIS	Snowmap; NDSI; multispectral enhancement; ARSIS; SnowFrac; Snowl; Aqua + Terra composite	Hall *et al.* (1995, 2002); Hall and Riggs (2007); Riggs and Hall (2004); Salomonson and Appel (2004, 2006); Klein and Barnett (2003); Parajka *et al.* (2010); Miller and Lee (2005); Sirguey *et al.* (2008); Vikhamar and Solberg (2002); Wang and Xie (2009)	500 m (250 m)	Daily, 8-day, monthly	~95% (clear sky) 31–45% (all weather conditions)	SC, SCF
Landsat	NDSI; Decision-trees; SnowFrac	Rosenthal and Dozier (1996); Vikhamar and Solberg (2002)	30 m	Every 16th day	$R^2 = 0.979$	SC, SCF
AVHRR	Snowcover; theta	Fernandes and Zhao (2008); Maxson *et al.* (1998)	1000, 5000 m	Daily	~87% (for 50% of test sites)	SC
MERIS+AATSR	Supervised fuzzy statistical classification	Pepe *et al.* (2005)	260 m*, 290 m	Every three days	95–98%	SC, SCF

(*Continued*)

Table 4. (Continued.)

Sensor(s)	Method(s)	Author(s)	Spacial resolution	Temporal resolution	Accuracy	Derived parameters
AMSR-E	SWEMAP	Chang and Rango (2000); Kelly (2009)	25 km	Daily, 5-day,	3.7 cm error	SWE, SD, SC
SMMR	Spectral gradient $(T_{b18} - T_{b37}) \times c$	Foster *et al.* (1996); Derksen (2008); Chang *et al.* (1987)	25 km	Daily, 5-day	2.2 cm; 1.5 cm error; $R^2 =$ 0.75–0.8	SWE, SD
SMM/I	Snow Emission Model-Based Automatic Inversion Algorithm	Pulliainen and Hallikainen (2001); Goïta *et al.* (2003); Derksen *et al.* (2003a,b)	25 km	Daily, 5-day	2.3 cm; 1.4–3.3 cm; 1.5 cm error	SWE, SD
MODIS+AMSR-E	Combination of products	Liang *et al.* (2008); Gao *et al.* (2010)	500 m	Daily	~85%	SC
MODIS	MODSCAG	Painter *et al.* (2009)	500 m	Daily	SC: 95%, Albedo: 95% Grain size error: 51 μm	SC, SCF, Albedo, Snow grain size
GOES+SSM/I	Combination of products	Romanov *et al.* (2000)	4 km	Every 30 minutes	~85%	SC
ATSR-2/AATSR	NLR and SCAmod	Solberg and Andersen (1994); Metsämäki *et al.* (2005)	0.01°	Daily	Comparable to MODIS snowmap results	SC, SCF
MODIS+AMSR-E+QSCAT	ANSA	Foster *et al.* (2011)	25 km	Daily	Better than the single base products	SC, SWE, SD, SCF, Snowmelt

$$\mathrm{NDSI} = \frac{b_4 - b_6}{b_4 + b_6}, \tag{1}$$

where b_4 and b_6 refer to MODIS bands 4 (0.54–0.56 μm) and 6 (1.62–1.65 μm), respectively (Hall *et al*. 2002). The NDSI was first introduced by Crane and Anderson (1984) for experimental Defense Meteorological Satellite Program (DMSP) data. Dozier (1989) used Landsat bands 2 (0.53–0.61 μm) and 5 (1.55–1.75 μm) in a similar study.

Because band 6 on Aqua MODIS is non-functional, NDSI(Aqua) is calculated using band 7 (2.10–2.15 μm). The correlation between MODIS bands 6 and 7 over land is high. However, the reflectance magnitude of band 7 is lower. Additionally, the spatial misregistration between bands 7 and 4 accounts for 0.3 pixels compared to a misregistration of only 0.1 pixels for bands 6 to 4 (Salomonson and Appel 2006).

$$\mathrm{NDSI(Aqua)} = \frac{b_4 - b_7}{b_4 + b_7}. \tag{2}$$

Riggs and Hall (2004) confirmed that switching the bands greatly improved the accuracy for the Aqua MODIS product. The snow patterns from Terra and Aqua MODIS are now very similar.

The NDSI is used to automatically distinguish between clouds and snow; while the reflectance of clouds remains high for MODIS band 6 (7 for Aqua), the reflectance of snow drops to near zero in this spectral region (Hall *et al*. 1995). To map snow extent automatically with NDSI, a threshold value of NDSI >0.4 is used to indicate snow coverage. This value has been suggested by Hall *et al*. (1995) after extensive analyses for the USA. Klein and Barnett (2003) validated daily MODIS snow-cover maps and proved that an NDSI value >0.4 indicates snow-covered surfaces. For forested areas, both underestimation and overestimation errors can occur. To prevent underestimation, the NDSI threshold must be decreased because forests tend to mask out snow-covered ground. Hall *et al*. (2002) found that NDSI values <0.4 also indicate snow if the normalized difference vegetation index (NDVI) is around 0.1. Snow tends to lower the NDVI, and an NDVI ~ 0.1 is therefore an indication of snow-covered forests even if NDSI <0.4 (Hall *et al*. 2002). To prevent overestimation, the reflectance in MODIS band 4 (Landsat TM band 2) must exceed 10% to be mapped as snow (Klein *et al*. 1998). This additional reflectance test is required because dark surfaces such as forests significantly reduce the reflectance values and therefore cause the denominator of the NDSI equation (1) to be quite small. Small increases in the VIS wavelengths would lead to NDSI values high enough to indicate snow (Klein *et al*. 1998, Hall *et al*. 2002). The Snowmap algorithm only works for pixels with at least a 50% snow-cover fraction (Hall *et al*. 2002). Trying to catch smaller subpixel fractions of snow can lead to the erroneous assignment of bright, snow-free surfaces as snow (Hall *et al*. 1995). Fractional snow mapping techniques described later in this section can improve these results (Salomonson and Appel 2004). The overall accuracy of the daily MODIS snow-cover product (MOD10A1) reaches 93% for clear-sky conditions, but it varies according to the land-cover type and snow conditions (Hall and Riggs 2007). The overall accuracy including all-weather conditions is lower, reaching 31% for Aqua (MYD10A1) and 45% for Terra (MOD10A1) MODIS daily products (Gao *et al*. 2010).

Rosenthal and Dozier (1996) presented a decision-tree based classification model to map snow cover and fractional snow cover from Landsat TM data. The method was developed for Landsat TM 5 scenes taken from 1983 to 1993 in the Sierra Nevada in California, USA. Within this decision-tree, a large number of threshold and ratio tests (21 terminal nodes for the full cloud classification tree) are accomplished to first identify cloud contamination. A second tree derives snow cover from the TM scenes with an additional 11 terminal nodes. Mainly, discrete threshold tests including TM bands 1, 2, 4 and 5 (Rosenthal and Dozier 1996) are used. This second tree decides whether a pixel is covered by snow, water or 'other' surface types. A subsequent regression tree estimates fractional snow cover; this step is explained later in this section. The accuracy of the decision-tree based classification of Landsat TM is similar to the one achieved with high-resolution aerial photography. A linear relationship between these snow-cover estimates has been detected with a determination coefficient $R^2 = 0.979$.

Snowcover is an algorithm developed by Fernandes and Zhao in the year 2008 especially for AVHRR data over the Northern Hemisphere (Zhao and Fernandes 2009). They used top-of-atmosphere (TOA) reflectance of AVHRR channels 1 and 2, NDVI, clear-sky surface broadband albedo, skin temperature (ST), solar zenith angle (SZA) and a cloud mask for their analysis. As ground truth, SD measurements were taken from both the Meteorological Service of Canada (MSC, 67 *in situ* sites) and the Historical Soviet Daily Snow Depth Version 2 (HSDSD, 260 *in situ* sites). Initially designed to be used with the 1 km AVHRR imagery, the Snowcover algorithm was also used to derive snow cover from 5 km AVHRR land grid cells. Three steps were performed to acquire the final snow-cover product: (1) temporal filtering and interpolation of each grid cell by an adaptive rank filter, (2) normalization of channel 1 to standard acquisition geometry and (3) snow detection. The temporal stability of each pixel is analysed per year for this snow detection step. Samples of snow-free and snow-covered surface temperature and NDVI time series are used to define the threshold that will be used for the final snow-cover classification. A pixel is classified as snow only if it is above the threshold for snow-free ground. The analysis of the whole time series of each pixel allows for the estimation of snow cover under clouds or cloud shadows as well. A final temperature threshold eliminates misclassification during summer and autumn months.

Snowcover is capable of producing snow-cover maps for 90% of the period from 1982 to 2008 over the Western Arctic. The accuracy reaches values of 87% for 50% of the test sites (Fernandes and Zhao 2008). Snowcover avails itself of the Single Pixel Aggregate Rating of Cloudiness (SPARC) routines to discriminate clouds from snow. Within this procedure, several tests including a brightness temperature test, a reflectance brightness test and a reflectance test are accomplished to derive the likelihood of cloud cover for each pixel (Khlopenkov and Trishchenko 2007).

The National Operational Hydrologic Remote Sensing Center (NOHRSC) used AVHRR data from the National Oceanic and Atmospheric Administration (NOAA) to map snow extent for North America with the multi-band snow classification algorithm theta. Each pixel of an input AVHRR scene is treated by theta as a vector quantity consisting of the selected bands. To map snow-cover extent, NOHRSC conducted two individual classifications, both connected to a user-defined reference vector. First, a three-space vector was initialized using AVHRR bands 3, 4 and 5 to identify clouds while, as a second step, AVHRR bands 1–4 were used to identify snow and cloud extent. To construct the final snow-cover classification, the results from the first step must be subtracted from the second step. The success of the theta algorithm

depends on the selected input bands and the reference vector. Assuming that suitable input parameters have been found, this method is capable of screening both cirrus and cumulus clouds, and besides that it distinguishes cirrus clouds above snow cover.

Mixed pixels, cloud shadow and the presence of forested areas may influence the effectiveness. Furthermore, the method is not fully automated because the user must set thresholds for both steps of cloud and cloud/snow classifications (Maxson *et al*. 1998).

Today, NOHRSC uses the Snow Data Assimilation System (SNODAS) with a snow mass and energy balance model as the major source of information. The snow model runs in steps of 1 hour and assimilates the estimates of the last 18 hours to produce a 30 arc second snow-cover product. Remotely sensed data are only incorporated to map the boundaries between snow and snow-free ground for cloud-free pixels (Barret 2003).

One limitation that is common to most of the products mentioned so far is their relatively coarse resolution. A pixel size of 500 m × 500 m may be inapplicable for local or small-scale snow-cover analysis. Sirguey *et al*. (2008) developed a method to improve the spatial resolution of MODIS in the context of snow-cover mapping. As a basis, the ARSIS concept (Amélioration de la Résolution Spatiale par Injection de Structures) was used to fuse MODIS channels with different spatial resolutions into one improved snow-cover product. ARSIS is a multi-scale method that constructs a high resolution for a low-resolution band from the information given by an additional high-resolution band (Ranchin and Wald 2000).

Because no panchromatic band is available, the high-resolution band that is the closest to the respective lower resolution channel was chosen for the transformation (MODIS $b_1 => b_3$ and b_4; MODIS $b_2 => b_5$, b_6, b_7). After the new 250 m MODIS channels were computed, corrections for the topography and atmosphere were conducted, and a linear constrained unmixing was also applied for eight endmembers to produce subpixel snow-cover information. As a result, significantly better snow-cover products were generated. Compared to a 15 m Aster reference image, the overall overestimation of the snow-covered area decreased from 4.1% to 1.9%, the mean absolute error decreased by 20% and the global quality index (Q, introduced by Wang and Bovik (2002) as a universal image quality index) increased by 3%. The number of endmembers limits the use of the procedure to smaller regions with known land-cover circumstances. On the other hand, the method is beneficial for environmental or hydrological implementations in steep terrain, where coarser resolutions may lead to significantly increased misinterpretations of snow cover and fractional snow cover (Sirguey *et al*. 2008).

Additional methods exist to map snow cover also from different sensors. Pepe *et al*. (2005), for example, researched the ability to use the two Envisat instruments, the Medium Resolution Imaging Spectrometer (MERIS) and Advanced Along Track Scanning Radiometer (AATSR), to monitor snow cover in Alpine regions. SPOT VEGETATION data can be used to map snow cover, as shown by Lissens *et al*. (2000) and compared to MODIS, as shown by Simic *et al*. (2004). The Interactive Multisensor Snow and Ice Mapping System (IMS) also derives snow cover on a global scale. Since 1999, daily products are available, whereas earlier these maps were generated on a weekly basis with much manual interaction (Helfrich *et al*. 2006). It is not possible to include all these approaches in this review. For a detailed description, the reader should refer to the individual authors.

3.2 *Fractional snow-cover algorithms*

Because binary information about snow cover can produce large uncertainties, especially within hydrologic runoff models, it is desirable to produce fractional snow-cover maps from medium resolution satellite data – in particular, during the accumulation or ablation period of snow, but also in forested areas such approaches are reasonable (Vikhamar and Solberg 2002, Salomonson and Appel 2004, 2006).

Rosenthal and Dozier (1996) used a regression tree to estimate fractional snow cover from Landsat TM data, and their results were as accurate as those obtained from aerial photography. Endmember selection or snow grain size, shape or SWE had no impact on the algorithm.

Topography-induced illumination differences have only little or no effect on the results. In summary, the regression tree tests whether a pixel in VIS wavelengths reflects more or less radiation than is defined by a given threshold. If it reflects more, the pixel will be assigned to a higher snow-cover fraction. The contrary is performed for the IR wavelengths; the higher the reflection, the lower the snow-cover fraction will be (Rosenthal and Dozier 1996).

A supervised fuzzy classification approach was used by Pepe *et al*. (2005) to estimate fractional snow cover from MERIS data. Based on an interactively chosen training sample, the probability of a pixel belonging to a respective land-cover class is derived. As a result, a soft classification map for each land-cover class is created containing a value that describes the likelihood of a pixel representing the respective land-cover class. Fisher and Pathirana (1990) showed that such soft classification maps can be used to estimate fractional land-cover information. The approach was not done in the context of snow cover and was arranged for Landsat 5 data, which is different in spatial and temporal resolution from other sensors usually consulted to map snow cover. One conclusion, however, was that land-cover classes with well-defined spectral behaviours can be estimated with a *comparatively* high accuracy ($r = 0.984$ for water, $r = 0.945$ for wetland). Land-cover classes with a wide variety of spectral signatures on the other hand provide poor correlations ($r = 0.472$ for built-up area, $r = 0.504$ for open area). Because snow cover is characterized by a very strict spectral behaviour (high reflectance with up to 90% in the VIS region, reflectance values near zero in the near IR region; see Hall and Martinec 1985, Pepe *et al*. 2005, Wang *et al*. 2005), the fractional snow-cover estimations derived from fuzzy classification results should provide good accuracy (Pepe *et al*. 2005).

Salomonson and Appel (2006) developed a method to retrieve fractional snow-cover information for Aqua MODIS satellite data. The 500 m MODIS snow-cover product was used as the source. To retrieve the snow-cover fraction within a MODIS pixel, a concurrent Landsat scene was used and registered to the same 500 m grid as MODIS. Every Landsat pixel was then classified as snow or snow-free ground, and the percentage of snow cover within each MODIS pixel (fractional snow cover) was generated. By comparing multiple such results, a relationship between fractional snow cover and NDSI was computed depending on the used satellite:

$$\mathrm{Fra6T} = -0.01 + 1.45 \times (\mathrm{NDSI}), \tag{3}$$

$$\mathrm{Fra7U} = -0.64 + 1.91 \times (\mathrm{NDSI}). \tag{4}$$

Here, 6 and 7 refer to the used bands in the calculation of NDSI, while T (Terra) and U (average of two combined relationships for Aqua) stand for the used satellite. The

performance of these algorithms has been tested using different Landsat 7 ETM+ scenes. The correlation coefficients were located between 0.88 and 0.94 with an RMSE between 0.07 and 0.15. Accuracy was similar for both Terra and Aqua MODIS, but with Terra having some slight advantages that may result from the misregistration of 0.3 pixels between Aqua MODIS bands 7 and 4. Possible improvements of the method include the use of land-cover and terrain information to adjust equations (3) and (4). Atmospheric correction may also further improve the accuracy (Salomonson and Appel 2006). The algorithm is included in the MODIS standard product and provides fractional snow cover in an operational way depending on the NDSI value of the respective pixel (Solberg *et al*. 2006).

Vikhamar and Solberg (2002) focused on the problem of decreased snow-cover detection accuracy in forested areas. A subpixel snow-cover mapping technique called SnowFrac was developed, which is based on a linear spectral mixture model (SnowFor). SnowFor simulates the pixel reflectance of forests. The signal that reaches the satellite sensor consists of a function from trees, snow, bare ground and irradiance. Each of these components describes a function itself; for example, trees are a function of density, species and chlorophyll content and bare soil is a function of rock or soil type and vegetation. Irradiance depends on the satellite position, incidence angle and sensor characteristics. This results in a large number of variables, but the SnowFor method uses additional inputs to limit their number. A digital forest-cover map and several endmember fractions are estimated by submodels prior to the run of the SnowFor model.

Depending on the predominant tree types, a general forest reflectance model is adjusted. In the case of this study for Norway, spruce, pine and birch were the most prevalent tree species. The modelled pixel reflectance therefore consists of the sum of the area proportions occupied by the respective tree type, snow or bare soil.

The additional submodels mentioned before are BirchMod, ShadMod and DiffusMod. BirchMod calculates the effective branch area of leafless birch trees as a function of tree height and also takes into account the solar elevation angle. ShadMod estimates the cast shadows on the snow cover caused by trees depending on the solar position. DiffusMod computes the amount of diffuse radiation that is shielded by the tree crowns and therefore does not reach the sensor. By unmixing the whole SnowFor model, the snow-cover fraction can be estimated once the other variables are known.

It was concluded that each additional submodel continuously improved the results. ShadMod brought the biggest improvements, increasing R^2 from 0.48 to 0.62 for birch forest (Vikhamar and Solberg 2002).

The MODSCAG (MODIS Snow-Covered Area and Grain size) model was developed and tested by Painter *et al*. (2009). It is capable of deriving fractional snow cover, grain size and snow albedo from MODIS data. A library of modelled snow endmembers is used as the input together with endmembers for rock, soil, vegetation and lake ice. MODSCAG now analyses the linear spectral mixtures for each combination of two or more endmembers from the library. Snow-covered area percentage and snow grain size are selected for each pixel according to the result of the linear spectral mixture analysis and the model that fits best for each endmember. Snow albedo can finally be determined using the snow-cover fraction and grain size of each pixel as input. Validation was derived using Landsat observations for the fractional snow-cover part while field measurements were available for grain size validation. Energy balance towers were used to assess the accuracy of the albedo estimates. The RMSE for fractional snow cover ranges from 1 to 13% with a mean RMSE of 5%. For grain size, the MODSCAG method constantly overestimates actual snow grain radii by an

MAE of 51 μm and a mean error of 30 μm (with mean actual snow grain size between 83 and 268 μm). For snow albedo, the MAE was 4.2% with a mean error of 3.6% (Painter *et al*. 2009).

In the context of the GlobSnow project funded by the European Space Agency (ESA), fractional snow-cover products are generated on a daily, weekly and monthly basis using Along Track Scanning Radiometer 2 (ATSR-2) and AATSR data (see table 1 for details) for the complete Northern Hemisphere (Solberg *et al*. 2010). The Simple Cloud Detection Algorithm (SCDA) developed by the Finnish Environment Institute (SYKE) is used to recognize clouds. Once clouds, water bodies and glaciers have been masked out, the snow-cover fraction is calculated using two algorithms, one for mountainous areas (>2° local slope) above the tree line (Norwegian Linear-Reflectance-to-snow-cover algorithm NLR; developed by the Norwegian Computing Centre) and another for open areas and forested regions (SCAmod; developed by the SYKE).

The NLR algorithm was developed for AVHRR data initially (Solberg and Andersen 1994). It uses only two endmembers (100% snow cover and 0% snow cover) for linear spectral unmixing to derive the snow-cover fraction. The C-correction method (Meyer *et al.* 1993) is used to correct for topographic effects.

The SCAmod algorithm was designed to be suitable for most optical sensors and first applied to AVHRR data (see Metsämäki *et al*. 2005 for details). In the context of GlobSnow, it uses AATSR/ATSR-2 bands 1 and 4 (see table 1) to derive fractional snow-cover information for non-mountainous regions. Before the algorithm can be applied, a transmissivity map must be generated that serves as a reference for 100% (dry) snow-covered conditions. Depending on this map, the snow-cover fraction for each pixel is calculated by a semi-empirical reflectance model using reflectance values for wet snow, forest canopy and snow-free ground as input parameters.

The accuracy of the fractional snow-cover product was evaluated against MODIS and Landsat snow maps. Good overall agreement was found for both analyses with GlobSnow overestimating snow-cover fraction especially in June. Besides, discrepancies were recognized at the border of the mountain mask that also forms the border between the two algorithms (NLR and SCAmod) where a smooth transition of the results was expected but not always achieved (Solberg *et al*. 2010).

3.3 *Algorithms to estimate snow cover below clouds from the reflective part of the spectrum*

Because cloud cover hinders an optical sensor from measuring surface reflectance, various methods have been developed to estimate ground conditions underneath clouds. For hydrological models, it is important to have daily gapless information about the snow-cover extent. Rango (1996) mentioned that there is a definite need to develop techniques for snow-cover mapping beneath clouds. This is why, especially in the field of snow mapping with remotely sensed data, so many methods have been developed to interpolate snow extent below cloud cover.

Snowl is an algorithm that determines the regional snow line based on the MODIS snow-cover product (Parajka *et al*. 2010). The mean elevation of all snow-covered pixels is opposed to all snow-free pixels. If a clouded pixel lies above the regional snow line, it can be stated as snow covered. Otherwise, it will be reclassified as snow-free.

This method is capable of decreasing cloud cover in a standard MODIS snow-cover product from 60 to 20%. If cloud cover is too large in proportion to the entire scene, this method will not work properly. The threshold that is used to determine whether a

scene can be processed by Snowl or not (because of too much cloud cover) determines the accuracy of the final result. This accuracy ranges from 48.7% to 81.5% depending on the cloud threshold (Parajka *et al*. 2010).

A method that combines both Terra MODIS and Aqua MODIS to reduce the impact of cloud obscuration is presented by Wang and Xie (2009). With their method, only ~2.5 days are needed to create a cloud-free snow extent from MODIS.

The resultant Aqua–Terra composite achieved an accuracy of 90% when compared with *in situ* measurements at 20 meteorological stations. On average, the snow-cover duration was 9 days higher than that suggested by the *in situ* data. This overestimation was due to the compositing technique that combined several days and therefore produced uncertainties. A second source for the overestimation may be the imbalance in scale that always exists when point-ground measurements are compared with pixel sizes of – in this case – 500 m × 500 m.

Similar approaches were undertaken by Wang *et al*. (2009a) and Parajka and Blöschl (2008) to combine Aqua and Terra MODIS snow-cover products.

Gafurov and Bárdoyy (2009) interpolated snow cover below clouds using six successive steps. Their methods are based on the MODIS daily snow-cover product, which is determined using the Snowmap algorithm, described earlier in this article.

In the first step, the snow-cover products from Terra and Aqua MODIS are combined according to the method of Wang and Xie (2009). The temporal combination of snow-cover information is the second step. Up to 2 days in the past and 1 day into the future or 1 day in the past and 2 days into the future are analysed for cloud-free classification results.

In the third step, the maximum and minimum elevations of snow cover are evaluated similar to the method described by Parajka *et al*. (2010) earlier in this section. This method was only used for scenes with less than 30% cloud cover because determination of snow lines can lead to the wrong results if too many pixels are obscured by clouds.

In step four, the snow condition of the four neighbouring pixels of each cloud covered pixel is analysed. If at least three of them are classified as snow, the centre pixel will also be classified as snow covered.

Step five is similar to step four; here the eight neighbouring pixels of each cloud-covered pixel are analysed. If a pixel is snow covered and a direct neighbour is obscured by clouds but has a higher altitude, the cloudy pixel is also considered to be snow covered. Qobilov *et al*. (2001) suggested an alternative implementation of this step; if a pixel or segment of pixels is cloud covered, the nearest cloud-free pixel with the same elevation, azimuth and slope angle is used as a replacement. They used this method for AVHRR-processing only (Qobilov *et al*. 2001).

In step six, the time series of each pixel for the whole snow season is analysed to determine the start date of snow accumulation and the end date of complete snowmelt. Cloud-covered pixels were then reclassified depending on the results of the time series analysis. The effects of short intermediate snow fall or melting are not respected. The sixth step automatically removes all remaining cloud-covered pixels and is therefore placed at the end of the processing chain.

To validate the results, several MODIS snow-cover products with little cloud cover were artificially filled with cloud cover from other, more clouded scenes. It was reasoned that step one, the combination of Terra and Aqua MODIS, produced the highest improvements. Step four eliminated the smallest amount of cloudy pixels, whereas step six revised most. The accuracy of steps two to five accounts for 90–96% if they are accomplished in the given order. The accuracy of step one was not evaluated

because it only depends on the accuracy of the snow classification results. Step six produced the lowest accuracy (78%) but removed the largest amount of clouds (Gafurov and Bárdoyy 2009).

3.4 *Identification of snow cover and SWE with PM sensors*

PM sensors are capable of mapping the surface beneath clouds and in darkness, and they are therefore valuable in the context of daily time series analysis. Especially when clouds are present for many consecutive days, interpolation techniques presented in §3.3 become uncertain. Additionally, PM data can provide useful information on snowpack properties such as grain size or liquid water content (Rott and Nagler 1995). Various sensors provide global coverage with PM imagery. Refer to table 2 for a detailed overview. The drawbacks of these sensors include their coarse resolution, the maximum SD of ~1 m that can be mapped, difficulties in mapping through precipitating clouds and the inability to map SD when snow is containing liquid water (Chang and Rango 2000, König *et al*. 2001, Josberger and Mognard 2002).

Clifford (2010) gives an overview of available PM sensors and methods to map SWE, which is defined as the mass of water included in the snowpack per area unit. In theory, the spectral gradient between different microwave channels is used as an indicator for SWE:

$$\mathrm{SWE} = c \times (T_{\mathrm{b18H}} - T_{\mathrm{b37H}}). \tag{5}$$

SWE is given in millimetres, T_{b18H} and T_{b37H} refer to the horizontally polarized brightness temperature of 18 GHz and 37 GHz microwave channels and c represents the slope of the linear fit: 4.8 mm K^{-1} (Chang *et al*. 1987). The brightness temperature at 37 GHz is prone to volume scattering of the snowpack whereas the frequency of 18 GHz is sensitive to the underlying surface. Volume scattering is the basic source of information for SWE as long as the snow is dry and not interspersed with liquid water, which would prevent volume scattering and lead to absorption of the microwaves (Tait 1998, Che *et al*. 2008).

Not only horizontal but also vertical polarization can be used to retrieve SWE, but as Armstrong and Brodzik (2001) showed, the vertical polarization overestimates SWE in areas of desert soil or frozen ground whereas horizontal polarization only underestimates in early winter. The snow density is presumed to be 300 kg m^{-3}, which is a representative estimate for mature snow in North America, although the density can range from 100 kg m^{-3} for freshly fallen snow to 500 kg m^{-3} for very old snow (Foster *et al*. 1996). In a similar way like SWE, the SD can be derived:

$$\mathrm{SD} = 1.59(T_{\mathrm{b18H}} - T_{\mathrm{b37H}}). \tag{6}$$

For the snow grain size, constant values of 0.3 and 0.5 mm are assumed. Because grain size and density are fixed, this method can be ranked as a static model. Foster *et al*. (1996) showed that the static algorithm from Chang *et al*. (1987) underestimates snow mass in North America by more than 50% for the period from December to March.

Other aspects limit the feasibility of SWE and SD retrievals; the snow grain size is an important factor that influences the PM signal. To achieve higher accuracy with SWE products, the evolution of the snowpack including its grain size and structure should be incorporated. Che *et al*. (2008) confirmed that a grain size of 0.3 mm would

result in a coefficient $c = 1.59$ for SD estimations (see equation (6)). However, a grain size of 0.4 mm would change the coefficient to $c = 0.78$ (Che *et al*. 2008).

A second point is the handling of vegetation. Not only forest fraction but detailed information about how vegetation interacts and influences microwave signals is required for better SWE estimations (Derksen 2008, Clifford 2010). Contrary to crystal size, the snow crystal shape has little to no influence on SWE and SD estimations from PM sensors, as shown by Foster *et al*. (1999). Derksen (2008) described how deep snowpacks with SWE values greater 120 mm can cause the measurements from the 37 GHz regions to become unreliable. Volume scattering does not increase after this point. Additionally, the 18 GHz frequency can be influenced by volume scattering itself at SD greater 30 cm (Markus *et al*. 2006). The 10 GHz frequency can compensate for this problem if available, but the resolution is usually coarser than in the 18 GHz region (see table 2).

The basis of SWE and SD estimations with PM data is always related to equations (5) and (6). These formally static approaches have developed during the years, leading to fundamental improvements. Josberger and Mognard (2002) used air temperature as an additional input to estimate snow metamorphism. Their method was tested for the Northern Great Plains in the USA, which are characterized by very flat terrain, only very sparse forested areas and a large number (285) of climate stations.

The analysis of T_{b19}–T_{b37} GHz gradient maps showed that the gradient stays near zero until the first snow occurs on the ground, which causes the gradient to increase. Abrupt changes in the gradient signal where the difference between the channels falls back to zero again indicate a warming event with liquid water arrival. These impacts of changing air temperature induced Josberger and Mognard (2002) to develop a temperature gradient index (TGI) that describes the grain size metamorphism of snow crystals within a snowpack. This index is defined as the temperature difference between the bottom and the top of the snow surface divided through the snow thickness for a whole snow season. The index is then correlated with the spectral gradient of the snow-covered area during the snow season, and the congruence was found to be quite high because the spectral evolution of the snow-covered area followed that of the TGI. Therefore by including the TGI, SD and SWE can be calculated from PM data and air temperature measurements.

Josberger and Mognard (2002) concluded that TGI can be used as an indicator for snow grain size metamorphism.

This conclusion was also used for the first development of the AMSR-E SWE Algorithm (SWEmap) that is utilized to produce daily, 5-day and monthly global snow storage index maps (Chang and Rango 2000). Because the vertical structure of a snowpack can consist of different layers of densities, grain sizes and underlying surface conditions, the upwelling microwave radiation can vary extremely. This is why a number of different snowpack profiles have been selected to create a database that can be used with a multi-layer perceptron (MLP) type artificial neural network.

Chang and Tsang (1992) describe the idea behind the neural network approach to map SWE; because the neural network must be trained before using, simulated SWE data are integrated into the network. The microwave brightness temperature is the only input layer to the network. One or more hidden layers are used to process the data and there is again only one output layer.

As a result, the sum of all input signals to a hidden layer is processed by the sigmoid function. A back-propagation algorithm is used to train the network. This

algorithm compares the results of the process with the training datasets included at the beginning.

The training of the network is done by calculating different combinations of the three input parameters: snow crystal size, snow density and SD. Snow temperature is fixed at 265 K, and three additional atmospheric models are included: Mid-latitude winter, sub-Arctic winter and Arctic winter atmospheres. Seven hundred and twenty sets of input–output pairs are generated out of these variables and used for training of the neural network.

SWEmap is then prepared to derive the SWE estimates. First, the attributes of the respective pixel are gathered, including snow classes, fractional forest cover, land use, elevation, probability of snow, SWE history and land–water mask. Second, a number of tests are conducted. A snow probability test determines whether the occurrence of snow is possible for a respective pixel or not by – amongst others – analysing snow frequency maps for the last 10 years. A surface temperature test is added, deciding whether the presence of snow is possible.

SWEmap consists of a number of tests again. First, the surface temperature derived from IR bands or even PM data are tested, which has a reported accuracy of 1.2–2.5°C for SSM/I data (Pulliainen *et al*. 1997). The AMSR-E imagery is then tested for precipitation followed by a wet snow test. Fractional forest cover is included in a last step to linearly fit the maximum albedo of a pixel depending on the forest fraction with values of 0.8 for no forest fraction and 0.2 for 100% forest cover within a pixel.

The algorithm for determining SWE from AMSR-E has evolved in recent years. Because the 18 GHz frequency is affected by volume scattering for deep snowpacks (Derksen 2008), the 10 GHz frequency can be used instead (Kelly 2009). Additionally, the 89 GHz frequency can be included to map shallow snowpacks in combination with the 23 GHz frequency from the AMSR-E sensor. Because the 89 GHz region is prone to atmospheric contamination, additional tests are required to ensure the reliability of the shallow snow detection (Kelly 2009).

Pulliainen and Hallikainen (2001) presented a study to retrieve regional SWE from PM observations in the Kemijoki drainage area in Finland. An algorithm called the Snow Emission Model-Based Automatic Inversion Algorithm was used to retrieve SWE, and the results were compared to conventional spectral and polarization difference procedures. The algorithm was developed at the Helsinki University of Technology (HUT) and will from now on be called the *HUT* algorithm.

HUT is an emission model-based iterative algorithm that takes into account the average SD, density and grain size of snow. The details of the model are described by Pulliainen *et al*. (1999). The emission behaviour of snow is a function of grain size, density and SWE. The brightness temperature of each pixel is also modelled depending on the forest fraction to take into account the loss factor of the canopy. Atmospheric transmissivity, soil emission contribution and the effect of multiple reflections between the soil–snow and snow–air boundaries are also modelled using additional methods developed by Pulliainen *et al*. (1993, 1997) and Ulaby *et al*. (1981). When compared with independent experimental data and tower-based experiments, *HUT* modelled results agreed well with *in situ* data. In comparison to SSM/I-derived brightness temperature, the *HUT* model predictions showed correlation coefficients of 0.82 for vertically (V) and 0.76 for horizontally (H) polarized frequencies. Only observations with a daily maximum temperature greater than 0°C were allowed. If all observations regardless of temperature were analysed, the accuracy decreased to $r = 0.79$ (V) and $r = 0.69$ (H).

Because the emission model was now validated to produce admissible results, *HUT* was finally used to retrieve SWE from SSM/I data. Three SSM/I channels were used in a modified inversion scheme instead of the original method that tried to fit the modelled brightness temperature into the seven SSM/I channels (this led to unsatisfactory results). The modified scheme used the differences between the channels and polarizations instead of the raw SSM/I brightness temperatures (37 GHz (V), 19 GHz (V) and 19 GHz (H) were used) and also included the snow grain size and the standard deviation of the SSM/I brightness temperatures (2 K as shown by Hollinger *et al*. (1990) who verified that SSM/I is a stable and well-calibrated microwave sensor).

The results from the Kemijoki drainage area in Finland for night-time observations during the winter of 1993–1994 showed that *HUT* produces reasonable results ($r = 0.93$) when compared to *in situ* data. When calculated for the midwinter seasons from 1993–1994 to 1997–1998, the correlation coefficient for *HUT* was 0.75 (for observations with temperatures less than 0°C) to 0.62 (all midwinter observations) and therefore better when compared to the results of conventional SWE retrieval methods.

That is why the authors conclude that the performance of the algorithm depends mainly on the weather conditions and that additional information such as near-surface air temperature could still improve the results. Data for snow characteristics would also be useful to replace the fixed values such as snow grain size and snow density (Pulliainen and Hallikainen 2001).

The *HUT* model is also incorporated in the GlobSnow project to estimate SWE values for the complete Northern Hemisphere for the years from 1979 until present. Daily, weekly and monthly products are generated from SMMR, SSM/I and AMSR-E data (Luojus *et al*. 2010b). The method applied for the GlobSnow product is described by Pulliainen (2006). By combining ground-based observations with spaceborne PM data, the accuracy of SWE and SD estimates improves significantly. The analysis of spaceborne PM data alone is subject to major restrictions as the brightness temperature saturates at large SD values. The new assimilation technique estimates snow grain size at the ground-based stations and determines SWE and SD values at these stations while interpolating (Kriging interpolation) between their locations (Pulliainen 2006).

Derksen *et al*. (2003a) compared 18 winter seasons of *in situ* data and SWE derived from PM instruments in Western Canada. For the years from 1978 to 1996, 5-day average SWE estimates derived from SSM/I and SMMR have been crosschecked with *in situ* data. In regions with small forest cover, the agreement between the different results was good, whereas in heavily forested areas or at times when the SD exceeded 75 mm, SWE was systematically underestimated. Interannual performance variability was also observed when the accuracy of different years was evaluated. Whereas during the winter season of 1991–1992, the mean bias error (MBE) was only ~5 mm, in the following season the MBE was nearly 25 mm (Derksen *et al*. 2003a).

Derksen *et al*. (2003b) also presented a method to combine SSM/I and SMMR data for Central North America to derive an SWE time series. There is only a 6-week overlap of this time series because the SMMR sensor only operated until August 1987 with SSM/I starting in June 1987. It is desirable to have consistent and comparable time series of SWE estimations, and this is why this study is focused on the comparison of the two sensors. SD data from climate stations served as *in situ* data and have been converted to SWE using an average snow density described by Brown (2000).

In summary, both SMMR- and SSM/I-derived SWE estimates showed a consistent relative agreement with *in situ* data with none of the sensors being more accurate

than the other. Both sensors underestimated SWE in heavily forested areas for more than 15 mm. However, the SMMR sensor was found to underestimate SWE values significantly stronger than SSM/I. It was demonstrated that SWE magnitudes calculated from SSMR brightness temperature differ from the ones derived from SSM/I and that this circumstance should be accounted for in order to evaluate longer time series of SWE metrics (Derksen *et al*. 2003b).

3.5 *Methods for snow derivation based on the combination of PM and reflective data*

Because PM data has the capability to estimate snow cover underneath clouds, advanced combination methods of both PM and optical data are desired (König *et al*. 2001, Simic *et al*. 2004, Liang *et al*. 2008). Data from optical and thermal sensors alone cannot provide cloud-free snow-cover information on a daily basis. A combination of these sensors with PM sensors is therefore most desirable (Romanov *et al*. 2000) and recommended (Rango 1996).

Romanov *et al*. (2000) presented a system for automated mapping of snow cover for North America with a combination of VIS and IR data from the Geostationary Operational Environmental Satellites (GOES) and PM data from SSM/I. As measurements in the medium IR region of the spectrum (MIR) were not available from geostationary satellites until the launch of GOES-8, attempts to map snow cover from these sources encountered serious difficulties. Since 1994, the MIR range measurements are available and have been used in this study to automatically map snow extent for North America.

The GOES observations are available every 30 minutes. By compositing these individual images using the pixel with maximum 11 μm brightness temperature and minimum MIR, cloud coverage is mitigated. To identify a snow-covered pixel, two steps are established after a water mask is applied to exclude all water bodies from the analysis; the ratio between the VIS and the MIR channels is calculated, producing a snow index SI that indicates snow cover. To eliminate the influence of iced clouds and semi-transparent cirrus clouds, which is the most challenging problem, an additional temperature threshold is applied. This threshold is based on the surface temperature forecast of the National Centers for Environmental Prediction (NCEP) regional operational Eta Model. Because these model estimations can also be erroneous, the threshold is decreased by 10 K. Additionally, the IR brightness temperature must be lower than 283 K for a pixel to be mapped as snow. In the second step, all snow-free pixels are now classified either as land or as cloud. If the IR brightness temperature is lower than 283 K and VIS or MIR reflectance is high (at least 25% for VIS, 10% for MIR), the pixel is classified as cloud. Otherwise, the pixel is assumed to be cloud free.

The compositing of multiple GOES observations per day minimizes cloud coverage but does not eliminate it. This is why SSM/I-derived snow-cover data are used additionally. The SSM/I snow-cover maps are provided by NOAA as an automatically derived product. The resolution of the SSM/I snow-cover dataset is 30 km and is remapped to 4 km GOES resolution. To prevent false classification near water, all pixels as close as 30 km to water bodies are excluded. Precipitating clouds can also cause misclassifications and therefore, 'no data' is assumed for SSM/I where such precipitation is acknowledged. In a case where neither SSM/I nor GOES provides useful results, the previous day's classification is used.

For validation, 1000 climate stations reporting SD from the US cooperative network are compared to the blended snow-cover product for the period from February to April 1999. The GOES clear-sky classifications produced the most accurate results with 88% correct interpretations. The SSM/I snow maps only provide 80%. The blended product of GOES and SSM/I is 3% better than SSM/I, leading to an overall accuracy of 85% (Romanov *et al*. 2000).

Gao *et al*. (2010) combined MODIS and AMSR-E and also added an additional cloud mitigation step by combining Aqua and Terra MODIS prior to AMSR-E fusion (see §3.3; Wang and Xie 2009 or Wang *et al*. 2009b). The overall cloud coverage of the MODIS products (60.0% for Aqua and 55.0% for Terra MODIS) was reduced to 47.8% by the combination of both Aqua and Terra MODIS. The 25 km pixels of AMSR-E were downscaled to 500 m. The SWE values from the original AMSR-E product were then recalculated using the actual number of snow-covered pixels taken from the fused MODIS snow-cover product. A linear distribution of SWE within the snow-covered pixels retrieved from MODIS was assumed, and the original SWE estimations were recomputed using

$$\mathrm{SWE_n} = \mathrm{SWE_0} \times 2\left(\frac{2500}{N_{\mathrm{snow}}}\right), \tag{7}$$

where $\mathrm{SWE_n}$ represents the new SWE value for the respective 500 m pixel, $\mathrm{SWE_0}$ refers to the AMSR-E 25 km SWE value and N_{snow} stands for the number of snow-covered MODIS pixels within the AMSR-E pixel. The scaling factor 2 is used because SWE data taken from NSIDC (in this case AE_DySno) is scaled down by the factor 2.

The accuracy of the combined product was tested for the region of Fairbanks and Upper Susitna Valley, Alaska, and found to be better than any of the original snow-cover datasets. When compared to *in situ* data for the period from 1 October 2006 to 30 September 2007, the snow accuracy of the merged snow-cover product reached 86% and is therefore much better than the combined Terra–Aqua MODIS snow-cover product (49%) and still slightly better than the AMSR-E snow accuracy (85%). The accuracy for the no-snow period was also better for the combined product (95%) when compared to the original datasets (55% for Aqua–Terra MODIS product, 94% for AMSR-E product). During snow accumulation, the accuracy increased by 12–16% (compared to AMSR-E), and during melting the increase was 1–38% (compared to AMSR-E). Even when compared to the blended product of Liang *et al*. (2008), who tested the combination of Terra MODIS and AMSR-E for China, the accuracy was higher (75.4% for Liang *et al*. 2008; 86.0% for Gao *et al*. 2010).

The accuracy of SWE estimations did not change significantly during the midwinter season for the combined product. This is because the 25 km AMSR-E pixels were completely filled with snow, and the linear redistribution to 500 m pixels did not have much impact. During transition periods in autumn and spring, however, the accuracy improved because the snow cover was thin, patchy and in some cases wet. The final conclusion was that the combined product of Aqua and Terra MODIS together with AMSR-E can improve snow cover and SWE estimations and that the product can contribute to hydrological and meteorological modelling (Gao *et al*. 2010). Liang *et al.* (2008) developed a similar method. They concluded that the combined snow-cover products of Terra MODIS and AMSR-E can improve the accuracy of daily snow-cover estimations. Hall *et al*. (2007) also concluded that the combination of the

MODIS snow-cover product with AMSR-E snow estimations will produce a higher accuracy than any of the original data alone for the Lower Great Lakes region in North America.

Foster *et al*. (2011) combined VIS, PM and scatterometer data to produce a single snow-cover dataset containing SWE, snow extent, fractional snow cover, snowpack ripening, onset of snowmelt and actively melting areas. The algorithm is called ANSA (Air Force Weather Agency/NASA Snow Algorithm). MODIS, AMSR-E and QSCAT data were included to provide daily datasets for the whole Earth. The use of scatterometer data differentiates between this new product and prior approaches. Some basic facts about how snow-covered areas affect scatterometer observations are presented in §2.3. The MODIS snow-cover product was the default to estimate snow extent because it provided the best accuracy under clear-sky conditions. For clouded pixels, AMSR-E was used to derive the snow extent. SWE was inherited from the AMSR-E SWE product version T08. The 89 GHz frequency was only included for clear-sky regions to prevent negative effects of atmospheric contamination. Diurnal amplitude variations of the 37 GHz and 19 GHz frequencies were analysed to identify the onset of snowmelt. Information about forest fraction was finally included to improve the PM accuracy. The QSCAT backscatter from the K_u band was used additionally to determine snowmelt onset and actively melting areas. The accuracy of the blended ANSA product was better than both MODIS and AMSR-E alone, and research efforts are now focused on an improved resolution of the product (Foster *et al*. 2011).

4. Discussion

The most prevalent methods to map snow cover with remotely sensed data were presented in §3. The possible fields of application and also the advantages and drawbacks of the particular methods will now be discussed. The Snowmap algorithm is used to produce MODIS snow-cover products at various temporal and spatial resolutions. Daily, 8-day and monthly products are available and have been validated by various researchers and for many different parts of the Earth. Klein and Barnett (2003) compared the MODIS snow cover with *in situ* snow telemetry (SNOTEL) data from NOHRSC for the Upper Rio Grande basin. The MODIS product achieved an overall accuracy of 94% (with 4.4% omission and 25.5% commission errors). Maurer *et al*. (2003) compared the MODIS product with station data from the Missouri River basin and the Columbia River basin. GOES and AVHRR snow-cover estimates from NOHRSC were used as well to evaluate the accuracy of the MODIS product, and it was found that the MODIS snow-cover product was more accurate than the NOHRSC product. Parajka and Blöschl (2006) evaluated the daily MODIS product for Austria using station data from 754 SD stations. The agreement of MODIS reached 95% for cloud-free days with the highest error rates in January (15%) and the lowest error in summer months (1%). Huang *et al*. (2011) tested the MODIS product for Northern Xinjiang, China, and again the overall accuracy reached 95% when compared to ground measurements and Landsat data. Nearly the same result was found by Simic *et al*. (2004) for Canada; accuracy was 93% compared to ground-truth data. All these accuracy values were calculated analysing clear-sky scenes. Under all-weather conditions the overall accuracy can decrease down to 31% for Aqua (MYD10A1) and 45% for Terra (MOD10A1) MODIS daily snow-cover products (Gao *et al*. 2010).

The Snowmap algorithm had similar problems for each analysis. In mountainous regions, snow cover is often underestimated if no digital elevation map (DEM) is used to adjust for local solar illumination (Dozier and Marks 1987, König *et al*. 2001, Jain *et al*. 2008). Jain *et al*. (2008) therefore prepared an aspect map from a DEM including eight classes for orientations. However, Parajka and Blöschl (2006) did not observe any significant influence of the topography on the MODIS snow-cover accuracy. A problem that was confirmed not only from Parajka and Blöschl (2006) but also from Simic *et al*. (2004) and Klein and Barnett (2003) is the lower accuracy during transition periods. In autumn when snow cover starts to accumulate or during spring when snow cover is melting, the accuracy of the MODIS product is affected by more fractional snow cover or decreased reflection of the snow surface due to impurity. Vegetation is the third parameter that may lead to a decreased accuracy of the MODIS snow-cover product. Maurer *et al*. (2003), Klein and Barnett (2003), Huang *et al*. (2011) and Simic *et al*. (2004) confirmed this behaviour, especially for forested regions. But scrubland also can influence the accuracy of the MODIS product, as Huang *et al*. (2011) described. Thin snow cover can also introduce serious underestimation of actual snow cover with accuracy values of only 5% for 1 cm, 15% for 2 cm, 28% for 3 cm and 56% for 4 cm of SD (Wang *et al*. 2008b).

Despite these problems, the MODIS snow-cover product processed by the Snowmap algorithm is the most accurate product these days. Only a few alternative products are available in a similar temporal and spatial resolution and for the whole Earth.

The fractional snow-cover product facilitated by the GlobSnow project covers the complete Northern Hemisphere for the years from 1995 until present. The daily, weekly and monthly snow maps are derived from ATSR-2 and AATSR data. Two different algorithms are utilized for both mountainous and plain terrain. This differentiates between the GlobSnow product and the MODIS algorithm. When compared to the MODIS snow-cover product, the agreement was quite high. GlobSnow was overestimating snow cover for mountains during June. Additionally, the transition zone between the results from the two algorithms is not smooth in some regions, leading to inaccurate discrepancies in these areas. The cloud detection (SCDA) does not work for cold and high cloud tops consistently. In some cases, clouds are mistakenly detected along the border between snow cover and snow-free ground (Solberg *et al*. 2010). The product is freely available and produced every 24 hours in near real time, making GlobSnow an alternative to the MODIS product. The coarser resolution of 0.01° and the less elaborate cloud detection may limit the usability when compared to MODIS. In depth, evaluation of the accuracy is required to clarify the advantages and weaknesses of the GlobSnow product. The forest transmissivity map that is required as an input by the SCAmod algorithm is based on the GlobCover land-cover map, which does not represent very dense and very sparse forests correctly. Snow-cover fraction for these land-cover types, especially in North America and Siberia, can therefore be underestimated (Solberg *et al*. 2010). The handling of mountainous areas with a unique algorithm may on the other hand yield higher accuracy for these regions. Additionally, the use of the SCAmod algorithm for plain terrain may produce better snow-cover results for forested regions than MODIS because the algorithm was initially designed especially for the boreal forest zone (Metsämäki *et al*. 2005).

SPOT-4 VEGETATION (VGT) snow maps are available every other day at 1 km resolution and since 1998. The overall accuracy of this product is 83% as has been tested by Simic *et al*. (2004) for Canada. Because the accuracy decreases to 41% for

snow-covered forested areas, the product is not suited for regions with extensive forest cover. The algorithm can be adjusted to the respective region of interest to increase the accuracy, as shown by Dankers and De Jong (2004). They used the red instead of the green band and changed the NDSI threshold. However, the original VGT-S1 product should be used with care. The algorithm (not included in this review) is therefore not recommended for use on a global scale but better suited for regional applications and after prior analysis of the correct thresholds and band combinations.

Snow maps derived from AVHRR data are an additional alternative to MODIS. AVHRR data are available since the early 1980s, providing a long-time series of daily observations. Two methods to process snow cover from AVHRR data were reviewed in §3: Snowcover and theta algorithms. The accuracy of Snowcover products has been evaluated by Fernandes and Zhao (2008) for the Western Arctic and identified as 87% for 50% of the test sites (67 sites provided by the MSC and 260 sites from the HSDSD 2). The theta algorithm was originally designed for North America (Maxson *et al*. 1998) but has been successfully transferred to Turkey by Akyürek and Sorman (2002). Theta was able to recognize most clouds and discriminate between clouds and snow, which is often a problem for AVHRR because of the sparse selection of available bands. The coarser resolution of AVHRR (∼1000 m compared to 500 m from MODIS) also leads to an increased uncertainty due to mixed pixels (Maxson *et al*. 1998). Additionally, the method is not fully automated because some thresholds must be set manually. When compared to unsupervised classification results using the Iterative Self-Organizing Data Analysis Technique (ISODATA), theta was more accurate for the eastern part of Turkey (Akyürek and Sorman 2002).

While for large-scale analyses of snow-covered areas the resolution of 500 m (or 1000 m for AVHRR and VGT) is sufficient, it may be too coarse for local investigations. In such cases, the ARSIS concept can be used to increase the resolution of MODIS to 250 m as shown by Sirguey *et al*. (2008). The resultant snow-cover product was more accurate than the 500 m product with the mean absolute error decreased by 20%. Because a large number of endmembers are needed for unmixing, this procedure can only be applied on a local scale due to increased computing time. However, the ARSIS concept is a good alternative for steep terrain where the 500 m product may be disturbed by serious misinterpretations (Sirguey *et al*. 2008).

In summary, it can be stated that the MODIS snow-cover product should be preferred where available. The accuracy of AVHRR is constantly lower, often underestimating snow-covered areas seriously (Molotch and Margulis 2008). Lower resolution and the smaller selection of available spectral channels are the main reasons for this fact. The lesser geo-location accuracy of AVHRR (±1000 m) when compared to MODIS (±250 m) adds to this circumstance (Butt and Bilal 2011). The GlobSnow product may serve as an alternative for MODIS. The coarser resolution, simple cloud detection and the lack of an intensive evaluation for different regions and snow-cover conditions of GlobSnow still put the MODIS product ahead. The IMS daily snow-cover maps have a coarser resolution (4 km). Although PM, station data and atmospheric models are used to generate cloud-free data, errors can be introduced, especially in the ablation phase and for thin, cloud-covered snowpacks (Helfrich *et al*. 2006). Frei and Lee (2010) compared the MODIS snow extent to the IMS snow-cover product and found that MODIS consistently achieved better accuracy.

The decision-tree based classification of Landsat data is an example of high-resolution snow products. Because Landsat observations are only available every

16 days and the thresholds can require much manual work to adjust for a new region of interest, this method is not intended to be used operationally. Once correctly adjusted, the accuracy of the decision-tree is very good ($R^2 = 0.979$; Rosenthal and Dozier 1996). This makes Landsat snow-cover maps an ideal ground-truth source for medium resolution products.

Mixed pixels of snow-covered and snow-free ground are often a source of over- or underestimation of actual snow cover from medium resolution data. Algorithms to estimate the snow-cover fractions from Landsat (Rosenthal and Dozier 1996), MERIS (Pepe *et al*. 2005) and MODIS (Salomonson and Appel 2006) were reviewed in §3. All these approaches lead to higher accuracy of snow-cover classification results. They usually require additional input data such as land-cover maps (Salomonson and Appel 2006) or even detailed information about the composition of forests including different tree types and density (Vikhamar and Solberg 2002). If such ancillary data are available, fractional snow-cover algorithms can add to the accuracy of snow-cover products. Hydrologic models such as snowmelt runoff simulations can benefit from fractional snow-cover information in particular (Bales *et al*. 2008). On the other hand, computing times and data volume are most likely to increase during these calculations.

Methods to estimate snow cover below clouds are presented in §3. Unlike the products derived from PM sensors, these methods use the combination of multiple acquisitions (Wang and Xie 2009), neighbourhood analysis (Gafurov and Bárdoyy 2009) or terrain-dependent rules (Parajka *et al*. 2010) to mitigate the impact of cloud cover. Additionally, a seasonal filter can be applied to eliminate even the final cloud proportion (Gafurov and Bárdoyy 2009). The quality of these methods varies. The combination of different observations yields the best accuracy because the snow-cover classification is produced from the actual Earth observations and not modelled like that from the other methods. The combination of Terra and Aqua MODIS allows for cloud-free observations every 2.5 days, whereas without this step, 8 days are required to acquire the same result (Wang and Xie 2009). Snowl is an algorithm that estimates snow cover below clouds according to the terrain elevation of cloud-free pixels. The accuracy depends on prior defined thresholds and ranges from 48.7% for a progressive approach to 81.5% for a conservative approach (Parajka *et al*. 2010).

For observations made from the reflective part of the spectrum, clouds turn out to be the most inhibiting factor regarding accuracy and reliability of the results. There are two major reasons for this problem. First, clouds obscure the surface and do not allow for surface condition estimations from optical sensors. This limits the capability of snow-cover detection algorithms and can cause high errors of omission, depending on the size of the cloud-covered area and the number of consecutive days the surface was obscured. Especially at the beginning and the end of the snow season, when conditions can change dramatically within few days, false interpretations of snow cover can occur. The second problem is linked to the likelihood of confusion between clouds and snow. Because the spectral signature of clouds and snow is similar, especially for the VIS part of the spectrum, these confusions cannot be foreclosed. The use of additional wavelengths from the IR region can mitigate the misclassification of clouds but still, misinterpretation can occur between clouds and snow.

Land cover constitutes an additional error source of snow mapping with optical sensors. Water bodies and lake ice can induce false snow-cover recognition. Forested regions, however, turned out to be the most inhibiting land-cover class. Depending on the density of the forests and to some degree also depending on the tree types, the underlying snow cover is obscured by the canopy and cannot be estimated from space.

Forests also tend to prevent the surface from direct sun insolation, conserving the enclosed snow from melting longer than the snow from the neighbouring unobstructed areas. Both facts tend to underestimate the actual snow extent. The low reflection of dark forests such as spruce can cause the NDSI to reach values similar to snow. This can lead to overestimation of snow extent if no threshold for VIS bandwidths is included.

Terrain conditions such as elevation, slope and aspect account for a third error source. In mountainous regions, different illumination effects can occur depending on both satellite and SZA. Snow distribution may also vary according to local wind regimes, leading to snow-free areas in the direct neighbourhood of snow accumulation zones. The use of a DEM can help to minimize these problems.

PM data can be used to calculate SD and SWE with high temporal resolution and for the whole Earth. Their ability to record data during darkness and cloud cover makes them a valuable tool in snow-cover mapping. Derksen *et al*. (2003b) presented a method to combine SMMR and SSM/I, which was problematic because acquisition periods of the sensors only overlapped for a short time (6 weeks). Algorithms to map SWE with AMSR-E ensure a gapless time series from 1978 till present. Because the individual sensors operate at different frequencies, resolutions and overpasses, the change between different sensors must be handled with care.

The first methods to map SWE and SD used a static model with fixed values for snow density (300 kg m^{-3}) and snow crystal size (0.3–0.5 mm). Only frequencies around 18 GHz as background and 37 GHz as scattering signal were incorporated, which created serious uncertainties (Clifford 2010). These algorithms have developed over time, leading to version T08 of AMSR-E as the latest product. By including 89 GHz for shallow snow detection and 10 GHz for SWE greater than 120 mm, the accuracy was improved. An additional test for snow temperature and information about the forest fraction of each pixel is also applied (Foster *et al*. 2011).

The GlobSnow SWE product is generated from SMMR, SSM/I and AMSR-E data and provides daily, weekly and monthly datasets from 1979 till present. The method used to derive SWE was chosen after testing several possible algorithms, including the AMSR-E standard algorithm (Kelly *et al*. 2003), the algorithm of Chang *et al*. (1987) and the methods from Derksen *et al.* (2003a,b). It was found that the algorithm of Pulliainen (2006) worked best when applied to the whole Northern Hemisphere. The Pulliainen algorithm (HUT) induced an RMSE of 43.2 mm for Eurasia, 29.8 mm for Finland and 24–77 mm for Canada (Luojus *et al*. 2010a). When the algorithms were compared against each other, the latest version of the AMSR-E operational SWE algorithm was not yet developed. Because this new version now includes methods for improved SWE detection under shallow and deep snowpack conditions, the comparison may have led to a different conclusion.

SWE and SD estimates derived from PM data are subject to various restrictions. The coarse resolution can introduce large uncertainties due to mixed pixel effects. Water bodies limit the significance of the product, as observed by Dong *et al*. (2005). Volume scattering of snowpacks saturates at SWE values greater than 120 mm (Derksen 2008) to 150 mm (Luojus *et al.* 2010b), leading to major underestimations of SWE for deeper snowpacks. Finally, forest cover can reduce the accuracy of SWE and SD estimations. Validation of these SWE and SD values is also a problem. To assess the accuracy correctly, at least nine-point measurements would be required for a 1° by 1° grid. An analysis for the Northern Great Plains gave proof that single-point measurements used as ground truth can imply error rates as high as 22 cm for SD.

Using ten test sites instead of only one, the error was reduced to 7 cm (Chang *et al.* 2005). Because dense station networks measuring SD are not available for the whole Earth, validation of SWE and SD derived from coarse resolution PM data may not be possible without extensive field campaigns. In some studies (e.g. Derksen 2008 with more than 25 km spacing between test sites; Kelly 2009 with only ~250 test sites scattered over the whole Earth), this problem could not be solved. Kelly (2009) reported RMSE values between 17 and 23 cm for SD, Derksen (2008) RMSE values of 27–35 mm for SWE, both derived from AMSR-E.

The combination of observations from different sensor types is suggested by several authors (e.g. König *et al*. 2001, Simic *et al*. 2004, Liang *et al*. 2008, Foster *et al*. 2011) as it can utilize the benefits of the respective sensors. Their individual drawbacks can often be mitigated at the same time. Liang *et al*. (2008) combined MODIS and AMSR-E and found that the overall accuracy of this blended product was much higher (75.4%) than for the Terra MODIS daily snow-cover product alone (33.7% for all-weather conditions). Similar results were found by Gao *et al*. (2010), who calculated even 86% overall accuracy for the blended MODIS–AMSR-E product, whereas the combination of only Aqua and Terra MODIS only yielded 49% accuracy. Foster *et al*. (2011) blended MODIS, AMSR-E and QSCAT data to produce a daily dataset of snow extent, SWE, snow-cover fraction and information about snowmelt on a global scale. The authors again concluded that the combined dataset was more accurate than MODIS, AMSR-E or QSCAT alone.

Existing spaceborne sensors do not have the capability to derive the whole bandwidth of snow-cover parameters from a single platform on their own. This is why the National Aeronautics and Space Administration (NASA) accomplished the Cold Land Processes Field Experiment (CLPX) from winter 2002 to spring 2003. Field data and airborne and spaceborne remotely sensed data were collected for the same regions. Multispectral, hyperspectral, passive and active microwave data have been acquired and can be accessed from the website of NSIDC (http://nsidc.org/data/clpx). These data serve as a basis for future algorithms and validations.

Different algorithms and products are presented and discussed. It depends on the region and research subject which of the methods should be preferred. In retrospect, it seems that snow-cover products blended from reflective, PM and maybe even scatterometer data are the best choice. The accuracy is higher than for the individual products and the bandwidth of the available snow-cover characteristics that can be determined is broader. In fact, these are conclusive arguments, and because the development of the combined algorithms has advanced during the recent years, they seem appropriate. However, the coarse resolution of the PM datasets can limit the usefulness of derived and combined products. Molotch and Margulis (2008) confirmed that PM data are not suited to small-scale analysis of SWE. The coarse resolution generalizes SWE in mountainous regions and can attenuate the SWE variations. Additional input data such as forest fraction maps and information about water bodies are needed. Additionally, the validation of blended snow products can be problematic depending on the region and availability of *in situ* data.

The 10 GHz frequency is not facilitated by the SSM/I sensor while the 89 GHz region was not included for the SMMR sensor. It depends on the location whether these frequencies are recommended or not. The 10 GHz data for example is not necessarily needed when SWE will not exceed 120–150 mm. However, the decision on which sensor to choose when relying on PM data should be easy. For the years before 1987, SMMR was the only available data source. From 1987 to 2002, SSM/I was the

only sensor to measure the Earth's surface in the PM region and after 2002, AMSR-E should be preferred because it provides a larger bandwidth of frequencies than SSM/I. A comparison between different SWE retrieval algorithms derived in 2009 suggested that the method developed by Pulliainen (2006) fits best on a global scale (Luojus *et al*. 2010a). Because the latest version of the AMSR-E SWE algorithm (Kelly 2009) was not included in this comparison, it cannot be assured that this assessment still applies. Further analyses are required here. For optical sensors, MODIS seems to be the best choice as it provides the highest resolution and accuracy among the available sensors. For the years before 2000, AVHRR should be used, which has been available since 1978. Methods to map snow extent from AVHRR have been developed by various researchers, and the data are freely available. SPOT VEGETATION (since 1998) or ATSR (since 1991 for ATSR-1) data may be an alternative, but they cover a shorter time span and cannot be accessed for free easily. The Snowcover algorithm developed by Fernandes and Zhao (2008) can be applied to the AVHRR data. Results have been demonstrated to be quite accurate, but the algorithm needs additional input data such as ST. The theta algorithm (Maxson *et al*. 1998) may also be used, but it requires manual intervention.

5. Summary and conclusions

The previous sections gave an overview of available methods and algorithms to map snow-cover characteristics from space using remotely sensed data. While at the beginning of the development much manual work had to be done to classify and delineate snow cover, automated algorithms can process various input data today. The methods include simple thresholds from single bands, band ratios or snow indexes such as NDSI, algorithms relying on the temporal stability of snow and methods that treat a multi-dimensional pixel as a vector to separate clouds and snow.

Which algorithm to choose is a decision that depends mainly on the available input data and research question. Based on the experiences and evaluations of the products, the MODIS snow-cover product processed by the Snowmap algorithm should be preferred amongst the datasets generated from the reflective part of the spectrum. This product has been validated by numerous researchers for many different regions and deemed to be highly accurate under clear-sky conditions.

Some methods require additional information such as water masks, land-cover classifications or a digital elevation model as input. These additional data prevent the algorithms from misclassifications of water bodies as snow. Additionally, knowledge about forest cover is helpful to adjust thresholds in snow-cover mapping. A DEM can be used to calculate aspect and slope that may be integrated in some methods to further increase the accuracy. Algorithms exist that combine data from different sensors (reflective, PM and/or SAR data), calculate the fractional snow cover for each pixel or estimate snow cover beneath clouds. Many problems can arise when snow-covered areas are being classified from remotely sensed data. The confusions that can occur between clouds and snow have been mentioned above. Forested areas can cause the algorithms to underestimate or overestimate the actual snow cover. When the SD is low, the impact of the land-cover type on snow mapping accuracy is larger than for deeper snowpacks. The overall accuracy of snow mapping algorithms thus degrades with decreasing SD. Furthermore, snow-cover onset and melting seasons are very dynamic, leading to recurring changes of surface conditions. Clouds can cause serious

misinterpretations during this time when it is not possible to use temporal filter techniques reliably over multiple days. Additionally, sea ice can mistakenly be classified as snow while mountains cause unstable melting and accumulation behaviour depending on wind speed and direction and different slopes and facings of hillsides. PM sensors are capable of screening surface conditions even through clouds and, besides that, they can estimate the SWE from space, making them a valuable tool for hydrologic analyses such as runoff predictions. The fact that dry snow scatters microwave radiation that is emitted from the surface is exploited here. The relatively coarse resolution and the inability to map SWE when wet snow is present limit the usefulness of PM data. Again, forested areas and water bodies can also cause errors. Algorithms to estimate SWE rely on the difference of the brightness temperature measured in frequencies between ~10 and ~90 GHz (depending on the sensor). Best results can be obtained by combining the whole set of available frequencies. Some parameters such as snow grain size and snow density are often included as fixed values. Such static approaches with fixed parameters can cause serious errors of up to 50% of actual SWE. Allowing the parameters to adopt for weather conditions and therefore changed grain size and density can improve the results. The inclusion of land-cover and fractional forest-cover maps further enhances the accuracy, leading to errors of 7–15 mm SWE in boreal forests.

The methods presented in this review are capable of characterizing snow-cover extent and SWE on a daily basis. The need for such products arises in the context not only of climate change but also for regional hydrological modelling and water availability predictions. Accuracies vary depending on the available satellite sensor, the chosen algorithms, the geography of the study site and the ancillary input data. Land-cover classifications, water masks and information about fractional forest cover are useful for most of the methods and lead to improved results. The chosen satellite data as well as the applied methods depend on the desired results and region; for regional snow-cover estimations (e.g. small catchments), Landsat data with a high spatial resolution may be chosen whereas for daily global snow-cover products, MODIS, AMSR-E or other PM sensors can be used.

The various problems and drawbacks of the different sensors and methods are also discussed. Although the development of snow-cover algorithms started already during the 1960s, there is still room for enhancements. New sensors are being brought into space, allowing for new methods or the adaption and combination of already existing ones. Because the problems linked with PM algorithms differ from the ones linked with algorithms from the reflective part of the spectrum, a combination of these sensor types is often intended to be helpful (König *et al*. 2001, Simic *et al*. 2004, Che *et al*. 2008, Liang *et al*. 2008). Including active microwave data further upgrades the bandwidth of snow-cover products, adding information about the onset of snowmelt and melting conditions. Methods combining reflective, passive and active microwave data are still being researched, but they already produce promising results.

Once the snow-cover classification is produced from remotely sensed data, many different applications are possible. The progress and impact of climate change can be studied, for example. Snow-cover extent and snow mass are both sensible to temperature changes. Methods from both the PM and the reflective part of the spectrum are the only source of information that is available over large areas and in high temporal resolution. Additionally, these methods are capable of analysing snow extent as well as SWE, which makes them an ideal tool to monitor potential changes. Furthermore, results from snow-cover analysis are useful for hydrological subjects (Foster *et al*. 2005, Sirguey *et al*. 2008) as they can be integrated into hydrologic models such as

the snowmelt runoff model (Pepe *et al*. 2005, Parajka and Blöschl 2006, Butt and Bilal 2011). The results obtained from these models can be utilized by hydroelectric companies, especially during the melting season (Solberg and Andersen 1994) or for the forecasting of flooding events (Zhao *et al*. 2009).

Acknowledgements

The authors thank the providers of the remote sensing data and the snow-cover products used in this article. In detail: the Land Processes Distributed Active Archive Center (LP DAAC), located at the US Geological Survey (USGS) Earth Resources Observation and Science (EROS) Center (lpdaac.usgs.gov) for providing Landsat 7 and Hyperion data; National Snow and Ice Data Center (NSIDC, http://nsidc.org/index.html) for providing the MODIS daily snow-cover product (MOD10A1 and MYD10A1) and AVHRR data; National Aeronautics and Space Administration (NASA) for providing MODIS data (http://modis.gsfc.nasa.gov/). The authors also thank Corinne Frey and Patrick Leinenkugel from the German Aerospace Center (DLR)/German Remote Sensing Data Center (DFD) for their final review and finally the four reviewers for their valuable comments.

References

Ackerman, S., Frey, R., Strabala, K., Liu, Y., Gumley, L., Baum, B. and Menzel, P., 2010, *Discriminating Clear-Sky from Cloud With MODIS*. MODIS Algorithm Theoretical Basis Document (MOD35), Version 6.1, pp. 1–120 (Madison, WI: Cooperative Institute for Meteorological Satellite Studies, University of Wisconsin).

Akyürek, Z. and Sorman, A.Ü., 2002, Monitoring snow-covered areas using NOAA-AVHRR data in the eastern part of Turkey. *Hydrological Sciences*, **47**, pp. 243–252.

Amlien, J., 2008, *Remote Sensing of Snow with Passive Microwave Radiometers. A Review of Current Algorithms*, Report No. 1019 (Oslo: Norsk Regnesentral).

Aoki, T., Aoki, T., Fukabori, M., Hachikubo, A., Tachibana, Y. and Nishio, F., 2000, Effects of snow physical parameters on spectral albedo and bidirectional reflectance of snow surface. *Journal of Geophysical Research*, **105**, pp. 219–236.

Aoki, T., Motoyoshi, H., Kodama, Y., Yasunari, T.J. and Sugiura, K., 2007, Variations of the snow physical parameters and their effects on albedo in Sapporo, Japan. *Annals of Glaciology*, **46**, pp. 375–381.

Armstrong, R.L. and Brodzik, M.J., 2001, Recent Northern Hemisphere snow extent: a comparison of data derived from VIS and microwave satellite sensors. *Geophysical Research Letters*, **28**, pp. 3674–3676.

Bales, R.C., Dressler, K.A., Imam, B., Fassnacht, S.R. and Lampkin, D., 2008, Fractional snow cover in the Colorado and Rio Grande basins, 1995–2002. *Water Resources Research*, **44**, pp. 1–10.

Barret, A., 2003, *National Operational Hydrologic Remote Sensing Center Snow Data Assimilation System (SNODAS) Products at NSIDC*, NSIDC Special Report 11 (Boulder, CO: National Snow and Ice Data Center).

Barry, R.G., Armstrong, R., Callaghan, T., Cherry, J., Gearheard, S., Nolin, A., Russel, D. and Zaeckler, C., 2007, Snow. In *Global Outlook for Ice and Snow*, United Nations Environment Programme (Ed.), pp. 39–62 (Herfordshire: Earthprint).

Bernier, P.Y., 1987, Microwave remote sensing of snowpack properties – potential and limitations. *Nordic Hydrology*, **18**, pp. 1–20.

Brown, R.D., 2000, Northern Hemisphere snow cover variability and change, 1915–97. *Journal of Climate*, **13**, pp. 2339–2355.

Butt, M.J. and Bilal, M., 2011, Application of snowmelt runoff model for water resource management. *Hydrological Processes*, **25**,pp. 3735–3747.

Chang, A.T.C., Foster, J. and Hall, D.K., 1987, NIMBUS-7 SMMR derived global snow cover parameters. *Annals of Glaciology*, **9**, pp. 39–44.

Chang, A.T.C., Kelly, R.E., Josberger, E.G., Armstrong, R.L., Foster, J.L. and Mognard, N.M., 2005, Analysis of ground-measured and passive-microwave-derived snow depth variations in midwinter across the northern Great Plains. *Journal of Hydrometeorology*, **6**, pp. 20–33.

Chang, A.T.C. and Rango, A., 2000, *Algorithm Theoretical Basis Document (ATBD) for the AMSR-E Snow Water Equivalent Algorithm*, Version 3.1, pp. 1–49 (Greenbelt, MD: NASA Goddard Space Flight Center).

Chang, A.T.C. and Tsang, L., 1992, A neural network approach to inversion of snow water equivalent from passive microwave measurements. *Nordic Hydrology*, **23**, pp. 173–182.

Che, T., Li, X., Jin, R., Armstrong, R. and Zhang, T., 2008, Snow depth derived from passive microwave remote sensing data in China. *Annals of Glaciology*, **49**, pp. 145–154.

Choudhury, B.J. and Chang, A.T.C., 1979, Two-stream theory of reflectance of snow. *IEEE Transactions on Geoscience Electronics*, **17**, pp. 63–68.

Clifford, D., 2010, Global estimates of snow water equivalent from passive microwave instruments: history, challenges and future developments. *International Journal of Remote Sensing*, **31**, pp. 3707–3726.

Crane, R.G. and Anderson, M.R., 1984, Satellite discrimination of snow/cloud surfaces. *International Journal of Remote Sensing*, **5**, pp. 213–223.

Dankers, R. and De Jong, S.M., 2004, Monitoring snow-cover dynamics in Northern Fennoscandia with SPOT VEGETATION images. *International Journal of Remote Sensing*, **25**, pp. 2933–2949.

Derksen, C., 2008, The contribution of AMSR-E 18.7 and 10.7 GHz measurements to improved boreal forest snow water equivalent retrievals. *Remote Sensing of Environment*, **112**, pp. 2701–2710.

Derksen, C., Walker, A. and Goodison, B., 2003a, A comparison of 18 winter seasons of in-situ and passive microwave-derived snow water equivalent estimates in Western Canada. *Remote Sensing of Environment*, **88**, pp. 271–282.

Derksen, C., Walker, A., Ledrew, E. and Goodison, B., 2003b, Combining SMMR and SSM/I data for time series analysis of central North American snow water equivalent. *Journal of Hydrometeorology*, **4**, pp. 304–316.

Domine, F., Albert, M., Huthwelker, T., Jacobi, H.-W., Kokhanovsky, A.A., Lehning, M., Picard, G. and Simpson, W.R., 2007, Snow physics as relevant to snow photochemistry. *Atmospheric Chemistry and Physics Discussions*, **7**, pp. 5941–6036.

Dong, J., Walker, J.P. and Houser, P.R., 2005, Factors affecting remotely sensed snow water equivalent uncertainty. *Remote Sensing of Environment*, **97**, pp. 68–82.

Dozier, J., 1989, Spectral signature of Alpine snow cover from the Landsat Thematic Mapper. *Remote Sensing of Environment*, **28**, pp. 9–22.

Dozier, J. and Marks, D., 1987, Snow mapping and classification from Landsat Thematic Mapper data. *Annals of Glaciology*, **9**, pp. 97–103.

Fernandes, R. and Zhao, H., 2008, Mapping daily snow cover extent over land surfaces using NOAA AVHRR imagery. In *Paper Presented at 5th EARSeL Workshop: Remote Sensing of Land Ice and Snow*, 11–13 February 2008, European Association of Remote Sensing Laboratories, Bern, Switzerland, pp. 1–8. Available online at: http://www.earsel.org/workshops/LISSIG2008/Fernandes_Paper.pdf

Fisher, P.F. and Pathirana, S., 1990, The evaluation of fuzzy membership of land cover classes in the suburban zone. *Remote Sensing of Environment*, **34**, pp. 121–132.

Foster, J., Hall, D., Chang, A., Rango, A., Wergin, W. and Erbe, E., 1999, Effects of snow crystal shape on the scattering of passive microwave radiation. *IEEE Transactions on Geoscience and Remote Sensing*, **37**, pp. 1165–1168.

Foster, J., Liston, G., Koster, R., Essery, R., Behr, H., Dumenil, L., Verseghy, D., Thompson, S., Pollard, D. and Cohen, J., 1996, Snow cover and snow mass intercomparisons of general circulation models and remotely sensed datasets. *Journal of Climate*, **9**, pp. 409–426.

Foster, J., Sun, C., Walker, J.P., Kelly, R., Chang, A., Dong, J. and Powell, H., 2005, Quantifying the uncertainty in passive microwave snow water equivalent observations. *Remote Sensing of Environment*, **94**, pp. 187–203.

Foster, J.L., Chang, A.T.C., Hall, D.K. and Rango, A., 1991, Derivation of snow water equivalent in boreal forests using microwave radiometry. *Arctic*, **44**, pp. 147–152.

Foster, J.L., Hall, D.K., Eylander, J.B., Riggs, G.A., Nghiem, S.V., Tedesco, M., Kim, E., Montesano, P.M., Kelly, R.E.J., Casey, K.A. and Choudhury, B., 2011, A blended global snow product using VIS, passive microwave and scatterometer satellite data. *International Journal of Remote Sensing*, **32**, pp. 1371–1395.

Frei, A. and Lee, S., 2010, A comparison of optical-band based snow extent products during spring over North America. *Remote Sensing of Environment*, **114**, pp. 1940–1948.

Gafurov, A. and Bárdoyy, A., 2009, Cloud removal methodology from MODIS snow cover product. *Hydrology and Earth System Sciences*, **13**, pp. 1361–1373.

Gao, Y., Xie, H., Lu, N., Yao, T. and Liang, T., 2010, Toward advanced daily cloud-free snow cover and snow water equivalent products from Terra–Aqua MODIS and Aqua AMSR-E measurements. *Journal of Hydrology*, **385**, pp. 23–35.

Goïta, K., Walker, A.E. and Goodison, B.E., 2003, Algorithm development for the estimation of snow water equivalent in the boreal forest using passive microwave data. *International Journal of Remote Sensing*, **24**, pp. 1097–1102.

Griffin, M.K., Hsu, S.M., Burke, H.K., Orloff, S.M. and Upham, C.A., 2005, Examples of EO-1 Hyperion data analysis. *Lincoln Laboratory Journal*, **15**, pp. 271–298.

Grody, N.C. and Basist, A.N., 1996, Global identification of snowcover using SSM/I measurements. *IEEE Transactions on Geoscience and Remote Sensing*, **34**, pp. 237–249.

Hall, D.K., Foster, J.L. and Chang, A.T.C., 1982, Measurement and modeling of microwave emission from forested snowfields in Michigan. *Nordic Hydrology*, **13**, pp. 129–138.

Hall, D.K. and Martinec, J., 1985, *Remote Sensing of Ice and Snow* (New York: Chapman & Hall).

Hall, D.K., Montesano, P.M., Foster, J.L., Riggs, G.A., Kelly, R.E.J. and Czajkowski, K., 2007, Preliminary evaluation of the AFWA-NASA blended snow-cover product over the Lower Great Lakes region. In *64th Eastern Snow Conference*, 28 May–1 June 2007, St. Johns, Newfoundland, Canada, pp. 1–6.

Hall, D.K. and Riggs, G.A., 2007, Accuracy assessment of the MODIS snow products. *Hydrological Processes*, **21**, pp. 1534–1547.

Hall, D.K., Riggs, G.A., Foster, J. and Kumar, S.V., 2010, Development and evaluation of a cloud-gap-filled MODIS daily snow-cover product. *Remote Sensing of Environment*, **114**, pp. 496–503.

Hall, D.K., Riggs, G.A. and Salomonson, V.V., 1995, Development of methods for mapping global snow cover using moderate resolution imaging spectroradiometer data. *Remote Sensing of Environment*, **54**, pp. 127–140.

Hall, D.K., Riggs, G.A., Salomonson, V.V., Digirolamo, N.E. and Bayr, K.J., 2002, MODIS snow-cover products. *Remote Sensing of Environment*, **83**, pp. 181–194.

Helfrich, S.R., McNamara, D., Ramsay, B.H., Baldwin, T. and Kasheta, T., 2006, Enhancements and forthcoming developments to the interactive multisensor snow and ice mapping system (IMS). In *63rd Eastern Snow Conference*, 7–9 June 2006, Newark, DE.

Hollinger, J., Peirce, J. and Poe, G., 1990, SSM/I instrument evaluation. *IEEE Transactions on Geoscience and Remote Sensing*, **28**, pp. 781–790.

Huang, X., Liang, T., Zhang, X. and Guo, Z., 2011, Validation of MODIS snow cover products using Landsat and ground measurements during the 2001–2005 snow seasons over Northern Xinjiang, China. *International Journal of Remote Sensing*, **32**, pp. 133–152.

Hyvärinen, O., Eerola, K., Siljamo, N. and Koskinen, J., 2009, Comparison of snow cover from satellite and numerical weather prediction models in the Northern Hemisphere and Northern Europe. *Journal of Applied Meteorology and Climatology*, **48**, pp. 1199–1216.

Jain, S.K., Goswami, A. and Saraf, A.K., 2008, Accuracy assessment of MODIS, NOAA and IRS data in snow cover mapping under Himalayan conditions. *International Journal of Remote Sensing*, **29**, pp. 5863–5878.

Josberger, E.G. and Mognard, N.M., 2002, A passive microwave snow depth algorithm with a proxy for snow metamorphism. *Hydrological Processes*, **16**, pp. 1557–1568.

Kelly, R., 2009, The AMSR-E snow depth algorithm: description and initial results. *Journal of the Remote Sensing Society of Japan*, **29**, pp. 307–317.

Kelly, R., Chang, A., Tsang, L. and Foster, J., 2003, A prototype AMSR-E global snow area and snow depth algorithm. *IEEE Transactions on Geoscience and Remote Sensing*, **41**, pp. 230–242.

Khlopenkov, K.V. and Trishchenko, A.P., 2007, SPARC: new cloud, snow, and cloud shadow detection scheme for historical 1-km AVHRR data over Canada. *Journal of Atmospheric and Oceanic Technology*, **24**, pp. 322–343.

King, M.D., Tsay, S.C., Platnick, S.E., Wang, M. and Liou, K.N., 1997, *Cloud Retrieval Algorithms for MODIS: Optical Thickness, Effective Particle Radius and Thermodynamic Phase*, MODIS Algorithm Theoretical Basis Document No. ATBD-MOD-05 MOD06 – Cloud Product (Washington, DC: NASA), pp. 1–83.

Klein, A. and Barnett, A.C., 2003, Validation of daily MODIS snow cover maps of the Upper Rio Grande River Basin for the 2000–2001 snow year. *Remote Sensing of Environment*, **86**, pp. 162–176.

Klein, A.G., Hall, D.K. and Nolin, A.W., 2000, Development of a prototype snow albedo algorithm for the NASA MODIS instrument. In *57th Eastern Snow Conference*, 17–19 May 2000, Sysacuse, NY, USA, pp. 143–158.

Klein, A.G., Hall, D.K. and Riggs, G.A., 1998, Improving snow-cover mapping in forests through the use of a canopy reflectance model. *Hydrological Processes*, **12**, pp. 1723–1744.

König, M., Winther, J. and Isaksson, E., 2001, Measuring snow and glacier ice properties from satellite. *Reviews of Geophysics*, **39**, pp. 1–27.

Lemke, P., Ren, J., Alley, R.B., Allison, I., Carrasco, J., Flato, G., Fujii, Y., Kaser, G., Mote, P., Thomas, R.H. and Zang, T., 2007, Observations: changes in Snow, ice and frozen ground. In *Climate Change 2007: The Physical Science Basis. Contribution of Working Group I to the Fourth Assessment Report of the Intergovernmental Panel on Climate Change*, S. Solomon, D. Qin, M. Manning, Z. Chen, M. Marquis, K.B. Averyt, M. Tignor and H.L. Miller (Eds.), pp. 337–384 (Cambridge and New York: Cambridge University Press).

Liang, T., Zhang, X., Xie, H., Wu, C., Feng, Q., Huang, X. and Chen, Q., 2008, Toward improved daily snow cover mapping with advanced combination of MODIS and AMSR-E measurements. *Remote Sensing of Environment*, **112**, pp. 3750–3761.

Lissens, G., Kempeneers, P., Fierens, F. and Van Rensbergen, J., 2000, Development of cloud, snow, and shadow masking algorithm for VEGETATION imagery. In *IEEE International Geoscience and Remote Sensing Symposium, Proceedings*, 24–28 July 2000, Honolulu, HI, pp. 834–836.

Lucas, R.M. and Harrison, A.R., 1990, Snow observation by satellite: a review. *Remote Sensing Reviews*, **4**, pp. 285–348.

Luojus, K., Pulliainen, J., Takala, M., Derksen, C., Rott, H., Nagler, T., Solberg, R., Wiesmann, A., Metsämäki, S., Malnes, E. and Bojkov, B., 2010a, Investigating the

feasibility of the GlobSnow snow water equivalent data for climate research purposes. In *IEEE International Geoscience and Remote Sensing Symposium*, 25–30 July 2010, Honolulu, HI, pp. 4851–4853.

Luojus, K., Pulliainen, J., Takala, M. and Lemmetyinen, J., 2010b, Snow Water Equivalent (SWE) product guide, European Space Agency Study Contract Report, ESRIN Contract 21703/08/I-EC.

Markus, T., Powell, D. and Wang, J., 2006, Sensitivity of passive microwave snow depth retrievals to weather effects and snow evolution. *IEEE Transactions on Geoscience and Remote Sensing*, **44**, pp. 68–77.

Massom, R.A. (Ed.), 1991, *Satellite Remote Sensing of Polar Regions: Applications, Limitations and Date Availability* (Boca Raton, FL: Lewis Publishers).

Mätzler, C., 1994, Passive microwave signatures of landscapes in winter. *Meteorology and Atmospheric Physics*, **54**, pp. 241–260.

Mätzler, C. and Wegmüller, U., 1987, Dielectric properties of fresh-water ice at microwave frequencies. *Journal of Physics D: Applied Physics*, **20**, pp. 1623–1630.

Maurer, E.P., Rhoads, J.D., Dubayah, R.O. and Lettenmaier, D.P., 2003, Evaluation of the snow-covered area data product from MODIS. *Hydrological Processes*, **17**, pp. 59–71.

Maxson, R.W., Allen, M.W. and Szeliga, T.L., 1998, Theta – image classification by comparison of angles created between multi-channel vectors and an empirically selected reference vector. Available online at: http://www.nohrsc.noaa.gov/html/papers/theta/theta.htm (accessed 3 November 2010).

Metsämäki, S., Anttila, S., Markus, H. and Vepsäläinen, J., 2005, A feasible method for fractional snow cover mapping in boreal zone based on a reflectance model. *Remote Sensing of Environment*, **95**, pp. 77–95.

Meyer, P., Itten, K.I., Kellemberger, T., Sandmeier, S. and Sandmeier, R., 1993, Radiometric correction of topographically induced effects on Landsat TM data in an Alpine environmentS. *ISPRS Journal of Photogrammetry and Remote Sensing*, **48**, pp. 17–28.

Miller, S.D. and Lee, T.F., 2005, Satellite-based imagery techniques for daytime cloud/snow delineation from MODIS. *Journal of Applied Meteorology*, **44**, pp. 987–997.

Molotch, N.P. and Margulis, S.A., 2008, Estimating the distribution of snow water equivalent using remotely sensed snow cover data and a spatially distributed snowmelt model: a multi-resolution, multi-sensor comparison. *Advances in Water Resources*, **31**, pp. 1503–1514.

Nghiem, S.V., Steffen, K., Neumann, G. and Huff, R., 2005, Mapping of ice layer extent and snow accumulation in the percolation zone of the Greenland ice sheet. *Journal of Geophysical Research*, **110**, pp. 1–13.

Nghiem, S.V. and Tsai, W., 2001, Global snow cover monitoring with Spaceborne Ku-band scatterometer. *IEEE Transactions on Geoscience and Remote Sensing*, **39**, pp. 2118–2134.

Painter, T. H., Rittger, K., Mckenzie, C., Slaughter, P., Davis, R.E. and Dozier, J., 2009, Retrieval of subpixel snow covered area, grain size, and albedo from MODIS. *Remote Sensing of Environment*, **113**, pp. 868–879.

Parajka, J. and Blöschl, G., 2006, Validation of MODIS snow cover images over Austria. *Hydrology and Earth System Sciences*, **10**, pp. 679–689.

Parajka, J. and Blöschl, G., 2008, Spatio-temporal combination of MODIS images – potential for snow cover mapping. *Water Resources Research*, **44**, pp. 1–13.

Parajka, J., Pepe, M., Rampini, A., Rossi, S. and Blöschl, G., 2010, A regional snow-line method for estimating snow cover from MODIS during cloud cover. *Journal of Hydrology*, **381**, pp. 203–212.

Peng, S., Piao, S., Ciais, P. and Fang, J., 2010, Change in winter snow depth and its impacts on vegetation in China. *Global Change Biology*, **16**, pp. 3004–3013.

Pepe, M., Brivio, P.A., Rampini, A., Rota Nodari, F. and Boschetti, M., 2005, Snow cover monitoring in Alpine regions using ENVISAT optical data. *International Journal of Remote Sensing*, **26**, pp. 4661–4667.

Pulliainen, J.T., 2006, Mapping of snow water equivalent and snow depth in boreal and sub-arctic zones by assimilating space-borne microwave radiometer data and ground-based observations. *Remote Sensing of Environment*, **101**, pp. 257–269.

Pulliainen, J.T., Grandell, J. and Hallikainen, M.T., 1997, Retrieval of surface temperature in boreal forest zone from SSM/I data. *IEEE Transactions on Geoscience and Remote Sensing*, **35**, pp. 1188–1200.

Pulliainen, J.T., Grandell, J. and Hallikainen, M., 1999, HUT snow emission model and its applicability to snow water equivalent retrieval. *IEEE Transactions on Geoscience and Remote Sensing*, **37**, pp. 1378–1390.

Pulliainen, J.T. and Hallikainen, M., 2001, Retrieval of regional snow water equivalent from space-borne passive microwave observations. *Remote Sensing of Environment*, **75**, pp. 76–85.

Pulliainen, J.T., Kärnä, J.P. and Hallikainen, M.T., 1993, Development of geophysical retrieval algorithms for the MIMR. *IEEE Transactions on Geoscience and Remote Sensing*, **31**, pp. 268–277.

Qin, D., Liu, S. and Li, P., 2006, Snow cover distribution, variability, and response to climate change in Western China. *Journal of Climate*, **19**, pp. 1820–1833.

Qobilov, T., Pertziger, F., Vasilina, L. and Baumgartner, M.F., 2001, Operational technology for snow-cover mapping in the Central Asian mountains using NOAA-AVHRR data. *Remote Sensing and Hydrology*, **267**, pp. 76–80.

Ranchin, T. and Wald, L., 2000, Fusion of high spatial and spectral resolution images: the ARSIS concept and its implementation. *Photogrammetric Engineering and Remote Sensing*, **66**, pp. 49–61.

Rango, A., 1996, Spaceborne remote sensing for snow hydrology applications. *Hydrological Sciences*, **41**, pp. 477–494.

Riggs, G.A. and Hall, D.K., 2004, Snow mapping with the MODIS Aqua instrument. In *61st Eastern Snow Conference*, 9–11 May 2004, Portland, ME.

Rodell, M. and Houser, P.R., 2004, Updating a land surface model with MODIS-derived snow cover. *Journal of Hydrometeorology*, **5**, pp. 1064–1075.

Romanov, P., Gutman, G. and Csiszar, I., 2000, Automated monitoring of snow cover over North America with multispectral satellite data. *Journal of Applied Meteorology*, **39**, pp. 1866–1880.

Rosenthal, W. and Dozier, J., 1996, Automated mapping of montane snow cover at subpixel resolution from the Landsat Thematic Mapper. *Water Resources Research*, **32**, pp. 115–130.

Rott, H., 1987, Remote sensing of snow. In *Proceedings of the Vancouver Symposium*, August 1987, IAHS Publication No. 166, pp. 279–290.

Rott, H. and Nagler, T., 1994, Capabilities of the ERS-1 SAR for snow and glacier monitoring in Alpine areas. In *Proceedings of the Second ERS-1 Symposium – Space at the Service of Our Environment*, 11–14 October 1993, Hamburg, Germany, ESA SP 361 (Paris: European Space Agency), pp. 965–970.

Rott, H. and Nagler, T., 1995, Intercomparison of snow retrieval algorithms by means of spaceborne microwave radiometry. In *Passive Microwave Remote Sensing of Land-Atmosphere Interactions*, B.J. Choudhury, Y.H. Kerr, E.G. Njoku and P. Pampaloni (Eds.), pp. 227–243 (Zeist: VSP).

Salomonson, V.V. and Appel, I., 2004, Estimating fractional snow cover from MODIS using the normalized difference snow index. *Remote Sensing of Environment*, **89**, pp. 351–360.

Salomonson, V.V. and Appel, I., 2006, Development of the Aqua MODIS NDSI fractional snow cover algorithm and validation results. *IEEE Transactions on Geoscience and Remote Sensing*, **44**, pp. 1747–1756.

Simic, A., Fernandes, R., Brown, R., Romanov, P. and Park, W., 2004, Validation of VEGETATION, MODIS, and GOES + SSM/I snow-cover products over Canada based on surface snow depth observations. *Hydrological Processes*, **18**, pp. 1089–1104.

Sirguey, P., Mathieu, R., Arnoud, Y., Khan, M.M. and Chanussot, J., 2008, Improving MODIS spatial resolution for snow mapping using wavelet fusion and ARSIS concept. *IEEE Transactions on Geoscience and Remote Sensing*, **5**, pp. 78–82.

Solberg, R. and Andersen, T., 1994, An automatic system for operational snow-cover monitoring in the Norwegian mountain regions. In *Proceedings of the International Geoscience and Remote Sensing Symposium*, 8–12 August 1994, Pasadena, CA, pp. 2084–2086.

Solberg, R., Koren, H. and Amlien, J., 2006, *A Review of Optical Snow Cover Algorithms*, Norwegian Computing Centre Note SAMBA/40/06 (Norway: Norsk Regnesentral).

Solberg, R., Wangensteen, B., Metsämäki, S., Nagler, T., Sandner, R., Rott, H., Wiesmann, A., Luojus, K., Kangwa, M. and Pulliainen, J., 2010, *GlobSnow Snow Extent Product Guide. Product Version 1.0*, European Space Agency Study Contract Report, ESRIN Contract 21703/08/I-EC.

Strozzi, T., Teatini, P. and Tosi, L., 2009, TerraSAR-X reveals the impact of the mobile barrier works on Venice coastland stability. *Remote Sensing of Environment*, **113**, pp. 2682–2688.

Sturm, M., Holmgren, J. and Liston, G.E., 1995, A seasonal snow cover classification system for local to global applications. *Journal of Climate*, **8**, pp. 1261–1283.

Tait, A., 1998, Estimation of snow water equivalent using passive microwave radiation data. *Remote Sensing of Environment*, **64**, pp. 286–291.

Ulaby, F., Moore, R. and Fung, A. (Eds.), 1981, *Microwave Remote Sensing*, vol. 1, pp. 237–245 (Reading, MA: Addison-Wesley).

Vikhamar, D. and Solberg, R., 2002, Subpixel mapping of snow cover in forests by optical remote sensing. *Remote Sensing of Environment*, **84**, pp. 69–82.

Vikhamar, D. and Solberg, R., 2003, Snow-cover mapping in forests by constrained linear spectral unmixing of MODIS data. *Remote Sensing of Environment*, **88**, pp. 309–323.

Wang, L., Derksen, C. and Brown, R., 2008a, Detection of pan-Arctic terrestrial snowmelt from QuickSCAT, 2000–2005. *Remote Sensing of Environment*, **112**, pp. 3794–3805.

Wang, X. and Xie, H., 2009, New methods for studying the spatiotemporal variation of snow cover based on combination products of MODIS Terra and Aqua. *Journal of Hydrology*, **371**, pp. 192–200.

Wang, X., Xie, H. and Liang, T., 2008b, Evaluation of MODIS snow cover and cloud mask and its application in Northern Xinjiang, China. *Remote Sensing of Environment*, **112**, pp. 1497–1513.

Wang, X., Xie, H. and Liang, T., 2009a, Development and assessment of combined Terra and Aqua MODIS snow cover products in Colorado Plateau, USA and Northern Xinjiang, China. *Journal of Applied Remote Sensing*, **3**, pp. 1–15.

Wang, X., Xie, H., Liang, T. and Huang, X., 2009b, Comparison and validation of MODIS standard and new combination of Terra and Aqua snow cover products in Northern Xinjiang, China. *Hydrological Processes*, **23**, pp. 419–429.

Wang, Z. and Bovik, A.C., 2002, A universal image quality index. *IEEE Signal Processing Letters*, **9**, pp. 81–84.

Wang, L., Sharp, M., Brown, R., Derksen, C. and Rivard, B., 2005, Evaluating of spring snow covered area depletion in the Canadian Arctic from NOAA snow charts. *Remote Sensing of Environment*, **95**, pp. 453–463.

Winther, J., Gerland, S., Örbaek, J.B., Ivanov, B., Blanco, A. and Boike, J., 1999, Spectral reflectance of melting snow in a high Arctic watershed on Svalbard: some implications for optical satellite remote sensing studies. *Hydrological Processes*, **13**, pp. 2033–2049.

Ye, H., Cho, H. and Gustafson, P.E., 1998, The changes in Russian winter snow accumulation during 1936–83 and its spatial patterns. *Journal of Climate*, **11**, pp. 856–863.

Zeng, Q., Cao, M., Feng, X., Liang, F., Chen, X. and Sheng, W., 1984, A study of spectral reflection characteristics for snow ice and water in the north of China. *Hydrological Applications of Remote Sensing and Remote Data Transmission*, **145**, pp. 451–462.

Zhao, H. and Fernandes, R., 2009, Daily snow cover estimation from Advanced Very High Resolution Radiometer Polar Pathfinder data over Northern Hemisphere land surfaces during 1982–2004. *Journal of Geophysical Research*, **114**, pp. 1–14.

Zhao, Q., Liu, Z., Li, M., Wei, Z. and Fang, S., 2009, The snowmelt runoff forecasting model of coupling WRF and DHSVM. *Hydrology and Earth System Sciences Discussions*, **6**, pp. 3335–3357.